Ocean Surface Salinity Response to Atmospheric River Precipitation in the California Current System®

LAUREN HOFFMAN,^a MATTHEW R. MAZLOFF,^a SARAH T. GILLE,^a DONATA GIGLIO,^b
AND ANIRUDDH VARADARAJAN^c

^a Scripps Institution of Oceanography, University of California, San Diego, La Jolla, California
 ^b University of Colorado Boulder, Boulder, Colorado
 ^c Department of Mechanical and Aerospace Engineering, University of California, San Diego, La Jolla, California

(Manuscript received 17 November 2021, in final form 5 May 2022)

ABSTRACT: Atmospheric rivers (ARs) result in precipitation over land and ocean. Rainfall on the ocean can generate a buoyant layer of freshwater that impacts exchanges between the surface and the mixed layer. These "fresh lenses" are important for weather and climate because they may impact the ocean stratification at all time scales. Here we use in situ ocean data, collocated with AR events, and a one-dimensional configuration of a general circulation model, to investigate the impact of AR precipitation on surface ocean salinity in the California Current System (CCS) on seasonal and event-based time scales. We find that at coastal and onshore locations the CCS freshens through the rainy season due to AR events, and years with higher AR activity are associated with a stronger freshening signal. On shorter time scales, model simulations suggest that events characteristic of CCS ARs can produce salinity changes that are detectable by ocean instruments (\geq 0.01 psu). Here, the surface salinity change depends linearly on rain rate and inversely on wind speed. Higher wind speeds ($U > 8 \text{ m s}^{-1}$) induce mixing, distributing freshwater inputs to depths greater than 20 m. Lower wind speeds ($U \leq 8 \text{ m s}^{-1}$) allow freshwater lenses to remain at the surface. Results suggest that local precipitation is important in setting the freshwater seasonal cycle of the CCS and that the formation of freshwater lenses should be considered for identifying impacts of atmospheric variability on the upper ocean in the CCS on weather event time scales.

SIGNIFICANCE STATEMENT: Atmospheric rivers produce large amounts of rainfall. The purpose of this study is to understand how this rain impacts the surface ocean in the California Current System on seasonal and event time scales. Our results show that a greater precipitation over the rainy season leads to a larger decrease in salinity over time. On shorter time scales, these atmospheric river precipitation events commonly produce a surface salinity response that is detectable by ocean instruments. This salinity response depends on the amount of rainfall and the wind speed. In general, higher wind speeds will cause the freshwater input from rain to mix deeper, while lower wind speeds will have reduced mixing, allowing a layer of freshwater to persist at the surface.

KEYWORDS: Ocean; Atmosphere-ocean interaction; Atmospheric river; Ocean models; Salinity; Precipitation

1. Introduction

Freshwater inputs from rainfall can have variable impacts on surface ocean salinity. Of particular significance is the impact on upper-ocean stratification, which has been shown to limit the penetration depth of wind mixing and thus the vertical distribution of atmospheric fluxes (Schmitt 2008; Chaudhuri et al. 2021; Thompson et al. 2019). This has larger implications for intensification of the global water cycle (SPURS-2 Planning Group 2015; Yu et al. 2020). The relative importance of factors that are known to impact the ocean's response to freshwater inputs is not well characterized, especially in the subtropics where studies are limited. Atmospheric rivers (ARs) are narrow, elongated plumes of strong poleward water vapor transport known to produce large amounts of precipitation over the ocean and land in

© Supplemental information related to this paper is available at the Journals Online website: https://doi.org/10.1175/JPO-D-21-0272.s1.

Corresponding author: Lauren Hoffman, lahoffma@eng.ucsd.

the California Current System (CCS) (Ralph and Dettinger 2012; Ralph et al. 2013). The impact of ARs on surface ocean salinity has received minimal attention to date. Previously, global seasonal salinity variations in the upper ocean have been attributed to runoff (in coastal regions), advection in the ocean, as well as evaporation and precipitation (Yu 2011). Ren and Riser (2009) found that among these, in the subarctic regions of the northeast Pacific (45°-50°N), precipitation was the largest contributor. However, they did not address the California Current System, where variations in salinity have been linked to variations in anomalous advection along the trajectories of the California Current, the Inshore Current, and the California Undercurrent on seasonal (Lynn and Simpson 1987), interannual, and decadal (Schneider et al. 2005) time scales. Therefore, to date, seasonal variations of salinity within the CCS have mainly been attributed to advection (Lynn and Simpson 1987; Schneider et al. 2005). Here we hypothesize that local precipitation in the CCS (including ARs) provides a significant contribution to seasonal freshening. Additionally, we hypothesize that precipitation from ARs impacts the surface ocean on shorter time scales and may be detectable by oceanographic salinity sensors in some conditions.

DOI: 10.1175/JPO-D-21-0272.1

This study uses a combination of observations and modeling with the aim of understanding the surface salinity response to ARs in the California Current System by characterizing (i) the ocean salinity response to precipitation over the duration of the wet season and (ii) the role of rain rate and wind speed in driving changes in upper-ocean salinity and stratification for characteristic AR events on event time scales. Section 2 reviews the background, section 3 describes the observational data and model used to carry out the study, and section 4 describes methods of analysis. Section 5 focuses on the results of (i) the seasonal response and (ii) the response on event time scales. Section 6 provides a discussion of the results and their implications for understanding the ocean's salinity response to precipitation. Last, section 7 wraps up the study with conclusions.

2. Background

a. Salinity variability in the California Current System

Surface salinity variability in the CCS is typically attributed to alongshore advection from the California Current (Lynn and Simpson 1987; Schneider et al. 2005). Situated 150-1300 km offshore, the California Current transports cool, fresh, nutrient-rich water southward. Within the coastal zone (0-150 km) there is a poleward flow of warm, saline, low-oxygen subtropical waters from the California Inshore Countercurrent (IC) (Bograd et al. 2001; Lynn and Simpson 1987). At the surface (upper 50 m), the IC has seasonality, with a poleward flow occurring in the winter and fall, and an equatorward flow in the spring and summer (Lynn and Simpson 1987; Rudnick et al. 2017b). Salinity increases toward the coast, implying that an increase in offshore flow would result in an increase in salinity offshore (Rudnick et al. 2017b). Additionally, in a study of the temperature and salinity extremes found in the CCS beginning in 2017, Ren and Rudnick (2021) concluded that the positive salinity anomaly was a result of advection and that different source waters were found in the California Current from 2017 to 2019. During the summer, the increased salinity at the coast is enhanced due to coastal upwelling of cold, saline waters from depth (Auad et al. 2011). Riverine runoff has been linked to salinity decreases off the coast of central California (Kudela and Chavez 2004; Johnson et al. 1999). While, as noted in the introduction, salinity variability in the CCS has previously been attributed to intrinsic ocean dynamics (Lynn and Simpson 1987; Schneider et al. 2005; Auad et al. 2011; Kudela and Chavez 2004; Johnson et al. 1999), atmospheric forcing such as local surface freshwater flux may also influence surface salinity and is investigated here.

b. Salinity response to precipitation

The response of the ocean to freshwater input is a function of rainfall, wind, background stratification, heat flux, and vertical velocity in the upper ocean (Drushka et al. 2016). Rainfall forms stably stratified upper-ocean layers, with lenses of fresher water of O(1-10) m thick. Changes in these freshwater lenses are driven by the interaction between buoyancy and

shear forces; they can persist from minutes to hours depending on factors such as wind-driven surface mixing, lateral advection, convective overturning during nighttime cooling, and internal and surface waves (Brainerd and Gregg 1997; Drushka et al. 2019; Price 1979; Tomczak 1995; Wijesekera et al. 1999). While most fresh layers disperse within a few hours, in some cases fresh layers have been shown to persist for tens of hours (Walesby et al. 2015). Long-lasting freshwater layers can inhibit turbulent vertical mixing and decrease exchanges between the mixed layer and the thermocline (Schmitt 2008). This can lead to the formation of diurnal warm layers (Webster et al. 1996), enhanced surface currents (Wijesekera et al. 1999), and the suppression of near-surface turbulent dissipation below lenses (Smyth et al. 1997). In addition, fresh lenses may provide unexpected regional variation of internal wave energy propagation, dissipation, and mixing in the thermocline (Schmitt 2008). While this work pertains to freshwater lenses rather than barrier layers (Soloviev et al. 2015), it is interesting to note that de Boyer Montégut et al. (2007) identified the presence of unexplained barrier layers off the California coast at 25°-45° latitude. This study may explain the mechanisms behind this previously unexplained phenomenon.

While the ocean salinity response to precipitation in the CCS has received little attention to date, there is a growing pool of research on the ocean's response to freshwater input in the tropics, as experiments involving surface salinity profilers (SSP) provide high-resolution measurements near the surface. Results from a SSP deployed in the western tropical Pacific in December 2011 indicate that the vertical salinity difference between 0.26- and 0.11-m depth has a cubic dependence on rain rate and is inversely proportional to wind speed (Asher et al. 2014). Other studies have shown a linear relationship between the vertical salinity gradient and maximum rain rate (Boutin et al. 2014; Clayson et al. 2019; Drucker and Riser 2014; Drushka et al. 2016, 2019). However, wind speed was not factored into all of these studies. In the cases where wind was taken into account, results from a one-dimensional general ocean turbulence model (GOTM) and measurements made in the intertropical convergence zone (ITCZ) in the eastern tropical Pacific during the second Salinity Processes in the Upper-Ocean Regional Study (SPURS-2) showed the maximum difference in salinity between 1- and 5-m depth and the surface to be inversely proportional to wind speed (Drushka et al. 2016, 2019). In this study, we focus on the subtropics, where studies to date have been limited.

c. Atmospheric rivers in the California Current System

ARs account for a substantial amount of the global water transport, especially at midlatitudes where they can supply more than 90% of meridional transport of atmospheric water vapor (Ralph and Dettinger 2012; Zhu and Newell 1998). ARs are characterized by high atmospheric water vapor content and heavy winds. Because they are associated with extreme precipitation on land and over the ocean, especially in coastal regions (Ralph and Dettinger 2012; Ralph et al. 2013), ARs often cause devastating flooding and play a large role in

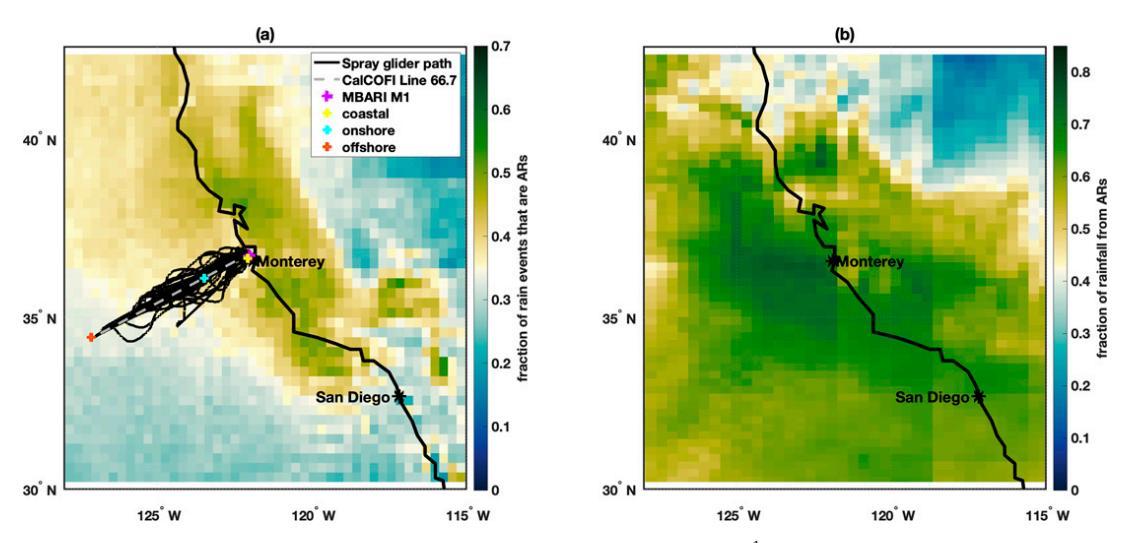


FIG. 1. (a) Fraction of rain events with precipitation greater than 5 mm day⁻¹ that are also ARs and (b) fraction of total precipitation that comes from ARs, within the region of the CCS. Events included occur between September and March for the years 2007–19. Also depicted is the trajectory traveled by CUGN Spray glider along CalCOFI line 66.7, the location of the MBARI M1 mooring (purple) and the coastal (yellow), onshore (cyan), and offshore (red) locations that were used during model analyses. The gray dashed line represents CalCOFI line 66.7 off the coast of Monterey, CA.

the global distribution of moisture and drought (Ralph and Dettinger 2011). ARs can occur in families consisting of several (typically 2-6) consecutive ARs (Fish et al. 2019), contributing to the accumulation of precipitation in the upper ocean and on land. The AR that extends from Hawaii to the U.S. West Coast carries moisture across the eastern Pacific to the coast of California. Off the coast of Monterey Bay in the CCS, 30%-48% of precipitation events greater than 5 mm day⁻¹ occur during ARs, which are responsible for up to 82% of total rainfall in the CCS, as seen along California Cooperative Oceanic Fisheries Investigations (CalCOFI) line 66.7 in Fig. 1, and as indicated by Guan and Waliser (2015). Argo profiles indicate large-scale upper-ocean freshening on average from December to February in areas of the Pacific that receive frequent AR-associated rainfall (Giglio et al. 2020). Implications of AR events for upper-ocean stratification and salinity are important, especially as climate projections indicate that the moisture content of ARs and the frequency of extreme AR events and storm seasons are expected to increase as a result of a warming climate (Dettinger 2011; Payne et al. 2020; Shields and Kiehl 2016).

d. Impacts of salinity on global moisture distribution

Changes in surface salinity have broad implications for the distribution of moisture and Earth's water cycle. For example, a reduction in sea surface salinity due to precipitation is hypothesized to lead to a positive feedback in which the formation of buoyant freshwater layers reduces vertical mixing in the upper ocean, which then contributes to increased SST, and in turn leads to a further increase in atmospheric convection and precipitation (SPURS-2 Planning Group 2015). In contrast, Williams et al. (2006) used climate modeling to show that freshwater lenses formed from an intensified hydrological

cycle could produce a basin-scale negative sea surface temperature feedback to anthropogenic human climate change. These nuances make understanding the vertical upper-ocean salinity gradient important for improving air-sea coupling in models (McCulloch et al. 2012) and understanding the role of upper-ocean stratification in a changing climate. Boutin et al. (2013) also suggested that the impact of precipitation on salinity stratification should be taken into account when assimilating satellite data under rainy conditions. Furthermore, the Clausius-Clapeyron relationship shows a strong, nonlinear dependence of water vapor pressure on temperature. With this relation, a rise in temperature of about 1°C leads to a 7% increase in vapor pressure, which causes changes in the water cycle as the vapor-carrying capacity of the atmosphere increases (Schmitt 2008). These changes will impact the global distribution of rainfall and drought, which is one of the most societally relevant aspects of climate change (SPURS-2 Planning Group 2015; Yu et al. 2020).

3. Observational data and model

A combination of observations and modeling are used to determine the seasonal and event-based response of ocean salinity to rain events within the CCS (30°-42.5°N, 128°-115°W). Here the region is divided into three subdomains based on the distance from shore: coastal (0–50 km), onshore (50–150 km), and offshore (150–550 km). The distance ranges are chosen based on the location of California Undercurrent (strongest around 70 km offshore), the California Inshore Countercurrent (strongest around 150 km offshore), and the California Current (strongest at 200–300 km offshore) as they fall along CalCOFi line 66.7 (Rudnick et al. 2017b). The subdomains include data collected along the Spray glider line, and their bounds, perpendicular to the coast, are indicated by

three colored markers in Fig. 1. Model initialization and forcing data are taken from observations and reanalysis fields at three coordinate locations (36.67°N, 122.06°W; 36.11°N, 123.47°W; and 34.43°N, 127.13°W, which are 30, 150, and 550 km offshore from Monterey Bay, respectively) within the three subdomains (coastal, onshore, and offshore). Figure 1 shows these locations and indicates the location of the Spray glider path along CalCOFi line 66.7 and the Monterey Bay Aquarium Research Institute (MBARI) M1 mooring location.

a. Instrument accuracy

The accuracy specification for conductivity–temperature–depth (CTD) instruments in measuring salinity is equivalent to 0.003 psu. However, this value is defined in a clean, well-mixed calibration bath and does not take into account effects of in situ ocean measurements. For example, the dynamic effects of moving instruments are known to increase errors in CTD measurements to 0.02–2.0 psu (Seabird Scientific 2016). This is consistent with observation errors for in situ salinity data that are found to be typically on the order of ± 0.01 psu after postprocessing for quality control (Vinogradova et al. 2019; Delcroix et al. 2005). These values are similar to the 0.01 psu accuracy reported in Argo salinity measurements after delayed-mode adjustments (Wong et al. 2020). Here, we use 0.01 psu as the threshold for a detectable salinity change.

b. ERA5

The ERA5 dataset is produced using a 4D-Var data assimilation of the European Centre for Medium-Range Weather Forecasts (ECMWF) Integrated Forecast System (IFS) by combining a vast number of historical observations into global estimates. Covering Earth on a 31-km (0.28128°) grid and resolving the atmosphere using 137 levels from the surface to 80-km height, the ERA5 dataset provides hourly estimates of a number of surface ocean and atmospheric variables from 1979 to present (Hersbach et al. 2020). In an analysis of the performance of five state-of-the-art global reanalyses in comparison to in situ data, ERA5 surface winds were found to have the best agreement with observed variability on daily and interannual time scales (Ramon et al. 2019). The ERA5 dataset showed significant improvements in precipitation estimates compared to ERA-Interim, with the caveat that biases still remained in the southeastern United States and on the North American western coast (Tarek et al. 2020). Additionally, reanalysis products (including the ERA5) showed the best agreement with precipitation measurements made by local ground stations in a comparison of a collection of satellite, reanalysis, and gauge measurements from the Frequent Rainfall Observations on GridS (FROGS) dataset for two case studies (California and Portugal) of extreme AR events (Ramos et al. 2021). However, the ERA5 often underestimated heavy precipitation compared to gauge measurements, with a mean absolute percent error of 68% (Ramos et al. 2021).

In this study, the ERA5 reanalysis dataset (Muñoz Sabater 2019) is used to characterize atmospheric conditions, i.e.,

atmospheric temperature, T_a (K); zonal and meridional wind speed, U_Z and U_M (m s⁻¹); downwelling longwave radiation and shortwave radiation, I_L and I_S (W m⁻²); specific humidity, SpH (kg kg⁻¹); evaporation minus precipitation, EmP (m s⁻¹); and rain rate, R (m s⁻¹). This study uses hourly data at the surface within the CCS from 2007 to 2019 to match the date range of the dataset for the Spray glider along line 66.7.

c. SIO-R1 AR catalog

The Scripps Institution of Oceanography (SIO)-generated AR catalog, the SIO-R1 AR catalog (Gershunov 2017), provides a record of AR activity on the North American west coast (20.0°-60.0°N, 160°-100°W). The dataset indicates whether or not an AR was detected (0 or 1) for each 6-hourly time step on a 2.5° resolution spatial grid (Gershunov et al. 2017). Here, this catalog is used to investigate the fraction of events with rainfall exceeding 5 mm day⁻¹ that are associated with ARs (Fig. 1), as well as the total number of AR events during the rainy season each year. Here we define the AR as "detected" if there is an AR in the grid cell or neighboring grid cell. To quantify rain events, we use ERA5 precipitation estimates at the AR locations.

d. CUGN spray line 66.7

The California Underwater Glider Network (CUGN) provides continuous sampling along CalCOFI line 66.7 by one Spray glider at a time (Rudnick 2016). The glider travels from Monterey Bay to a distance about 500 km offshore, vertically profiling in a sawtooth pattern. Each cycle to 500-m depth and back to the surface covers 3 km of horizontal distance and takes roughly 2.75 h. The quality controlled Spray glider dataset provides temperature and salinity observations from the glider ascent phase at discrete 10-m vertical levels, with the shallowest measurements available at 10-m depth (Davis et al. 2008). Finer resolution (raw) data are available, but performing quality control at depths shallower than 10 m is beyond the scope of this study. Salinity collected by the Spray glider is reported in practical salinity units (psu). Data are available from April 2007 through present (Rudnick et al. 2017b). Here glider data are used to characterize the ocean's salinity response to atmospheric precipitation on seasonal time scales and to initialize model runs (as described in sections 4a and 4b). Spray glider data allow us to investigate precipitation impacts on salinity at larger spatial scales over the CCS. One limitation of the Spray dataset for this study is that the temporal response of the upperocean salinity to precipitation is not fully captured at a particular location due to the fact that the glider is neither a Lagrangian nor an Eulerian platform and is traveling cross shore.

e. MBARI M1 mooring

The MBARI M1 mooring (Chavez 2015) measures continuously at one location. Therefore, in comparison to Spray, it has the disadvantage of conveying no spatial information, but the advantage of not aliasing spatial variability into temporal fluctuations. Here we use surface measurements

(nominal depth of 1 m) of ocean salinity at a location 20 km offshore of Monterey Bay (36.75°N, 122.0°W; purple marker in Fig. 1) from 2007 to 2019. This dataset is used to investigate the seasonal response of salinity to precipitation, to compare to model output, and to make event composites.

f. MITgcm 1D model

In this study, a one-dimensional configuration of the MITgcm (Adcroft et al. 2018), with vertical transport equations for momentum and heat, is used to run both seasonal (September–March) and event-based simulations (4-day sensitivity studies and 9-day case studies) aimed at characterizing the ocean's response to precipitation from ARs on different time scales. The MITgcm uses the nonlocal *K*-profile parameterization (KPP) vertical mixing scheme of Large et al. (1994) with a standard configuration as listed in Adcroft et al. (2018). Turbulent heat fluxes are computed in the model using methods from Large and Pond (1982). Details of model setup for each experimental run (seasonal, event sensitivity, and event case studies) are provided in Table 1 and in the sections that follow.

4. Methods

a. Seasonal time scale

1) OBSERVATIONAL METHODS

The seasonal response of ocean salinity is first investigated by looking at the MBARI M1 mooring surface (1 m) salinity measurements from 2015 to 2018, which are compared with model output from simulations run at the mooring location. Model forcing and initialization are discussed further in section 4a(2). This is followed by analysis of the annual and interannual (2008 through 2019) salinity anomaly from the Spray glider along line 66.7 in the CCS. As part of this analysis, we assess a one-dimensional salinity budget at a location 15 km offshore along the glider path using the hypothesis that changes in salinity within the water column will be fully explained by E-P in the form of an equation,

$$\frac{d}{dt} \left(\frac{\int_{0}^{Z} S \, dz}{Z} \right) = \frac{(E - P)S_{\text{ref}}}{Z}.$$
 (1)

Here we ignore advection and diffusion and calculate the amount of precipitation required to produce the rain-year salinity anomaly over a depth Z, in the limiting case where evaporation E (from ERA5) and rain P are the only contributing factors.

Additionally, over the rain-year from September through March, cumulative precipitation is calculated from ERA5 and compared with change in salinity at 10-m depth from the Spray glider along line 66.7 in coastal, onshore, and offshore regions. Glider offshore distance is calculated by comparing Spray glider data for latitude and longitude at given time steps with the initial coordinate location 5 km offshore. Salinity data are binned monthly and into coastal, onshore, and offshore subdomains for each year, and averaged over each bin. Changes in salinity from September (start of the rain-year) to

March are calculated for each year from the averages of the binned values. Along the line 66.7 glider path, ERA5 precipitation data are extracted at the fixed locations used to represent the coastal, onshore, and offshore regions, respectively (Fig. 1). ERA5 data from each location are binned by month to calculate cumulative monthly precipitation, from which cumulative precipitation is calculated from September through March, to be compared with change in salinity. Uncertainties for salinity and rainfall between September and March are computed by calculating the standard error of the mean in each bin and then propagating errors through the calculations to produce cumulative rainfall or salinity differences.

2) MODEL SETUP

The seasonal, one-dimensional MITgcm model is run over a period of 213 days (1 September-1 April) with a 0.5-h time step. Atmospheric forcing is applied daily and taken from ERA5 daily mean (longwave and shortwave radiation, zonal and meridional winds, atmospheric temperature, and specific humidity) and daily cumulative (precipitation) values. Forcing is applied for three different locations representing the coastal, onshore, and offshore subdomains. Initial conditions are taken to be temperature and salinity depth profiles, interpolated to 0.5-m intervals, from the Spray glider dataset along line 66.7, which provides measurements at 10-m intervals. The shallowest Spray measurements are at 10 m, so T and S between 0 and 10 m are set to the 10-m values, under the assumption of a well-mixed surface layer with constant T and S in the upper 10 m. Profiles of T and S are binned by month and by offshore distance for each year. Initial profiles are set as the calculated average profiles in September for each year (2008-19) and offshore distance regime. When no data are available for September in a given year/distance bin, the T and S profiles from October are used as initial conditions. This is the case for 2008 (coastal bin), 2012 (coastal and onshore bins), and 2017 (coastal bin). The model is run for the upper 140 m of the water column, using 280 vertical levels with 0.5-m spacing. The depth of 140 m was chosen to allow ample room for the downward propagation of the salinity response, as even for cases of high wind speeds, the salinity response to freshwater input was not found to propagate below 120-m depth. These model parameters are also listed in Table 1.

3) MODEL VALIDATION

The use of a one-dimensional model will allow for analysis without the influence of ocean processes such as horizontal advection, upwelling, and runoff, thus isolating the impact of rainfall and wind speed on upper-ocean salinity changes. We validate the model for long-term studies by comparing the observed and modeled March-minus-September salinity differences for all rain rates over the years 2008–19 (Fig. 2). To do this, the methods discussed in section 4a(1) for Spray glider data are applied to model output. A linear regression of observed to modeled salinity difference finds a slope of 1.25 with an r^2 value of 0.52, which is statistically significant at the 99% level. Figure 2 also shows that a 1:1 ratio between observed and modeled data falls within the 99% prediction interval

TABLE 1. Model parameters for seasonal, event sensitivity, and event case studies.

Study time scale	Seasonal	Event sensitivity	Case studies
Model parameters			
(one-dimensional MITgcm))		
Time step (s)	1800	60	60
Run time (days)/number of time steps	213/10 244	4/5760	9/13 020
Depth (m)/ dZ (m)	140/0.5	140/telescoping	140/telescoping
External forcing input interval (s)	86 400	60	3600
Number of runs	13 (September–March 2008–19)	36 (six rain rates/six wind speeds)	5 (16 Oct 2016, 27 Nov 2016, 11 Dec 2016, 19 Jan 2017, 17 Feb 2017)
Initial conditions (from Spray)			
Salinity profile	Averaged over September for each year within each offshore distance regime (coastal, onshore, offshore)	Constant from salinity average over five coastal AR events at 10 m depth, telescoping depths	Salinity on event start date at coastal location, interpolated to telescoping depths
Temperature profile	Averaged over September for each year within each offshore distance regime (coastal, onshore, offshore)	Temperature average over five coastal AR events, interpolated to telescoping depths	Temperature on event start date at coastal location, interpolated to telescoping depths
External forcing (from ERA5)			
Rain rate	Daily cumulative	Idealized 12-h Gaussian pulse $(0, 2, 3, 4, 5, \text{ and } 8 \text{ mm h}^{-1})$	Hourly
Wind speed	Daily mean	Idealized constant over four days (0, 2, 4, 8, 12, and 16 m s ⁻¹)	Hourly
Atmospheric temperature, specific humidity, and shortwave and longwave radiation	Daily mean	Constant (T_a , 13.1°C; SpH, 0.008 kg kg ⁻¹ ; I_s , -106.3 W m ⁻² ; I_L , -323.2 W m ⁻²), average over five AR events at the coastal location	Hourly

(green shading) and is close to the upper bound of the 99% confidence interval (blue shading) for the linear fit. Here the prediction interval represents the estimated range of a future observation, while the confidence interval represents the range of values for the linear regression slope and indicates how well this slope has been determined. Higher cumulative rainfall in Fig. 2 typically corresponds to a larger rainy-season decrease in salinity, as seen in the gradient of the color-coded data points, where large negative salinity differences (salinity decrease) are dark blue (high cumulative rain), and large positive salinity differences (salinity increase) are tan (low cumulative rain). Spray salinity differences tend to be larger than model differences, indicated by the slope being slightly large than one (i.e., for every 1 unit change in modeled salinity difference, Spray measures a change of 1.25 units). This difference in slope could be indicative of the model not including horizontal advection, upwelling, or runoff.

b. Event studies

1) OBSERVATIONAL METHODS

To assess the salinity response to precipitation on an event basis, we analyze ERA5 precipitation at the location of the MBARI M1 Mooring surface salinity measurements. Event composites are created by averaging rainfall, wind speed, and salinity from 85 heavy rain events as a function of time relative to the start date, described below. Events are included if daily cumulative precipitation is greater than a threshold of 5 mm and there has not been another rain event of this size within 10 days prior to the event start date. Events are defined to start (day 0) on the first date with rainfall exceeding the threshold. For the MBARI M1 mooring, events are chosen within a date range from January 2007 through March 2019. Composite analysis is not carried out using data from the Spray glider. While the decrease in salinity in response to precipitation is visible for a few glider events (not shown), the motion of the Spray glider makes composites too difficult to compute in a consistent way.

2) MODEL SETUP, SENSITIVITY STUDIES

Event-based sensitivity studies are run in the one-dimensional configuration of the MITgcm for 4-day periods to study the impact of AR events on the formation of freshwater lenses. Atmospheric forcing is applied every minute with the 60-s time steps linearly interpolated from hourly ERA5 fields.

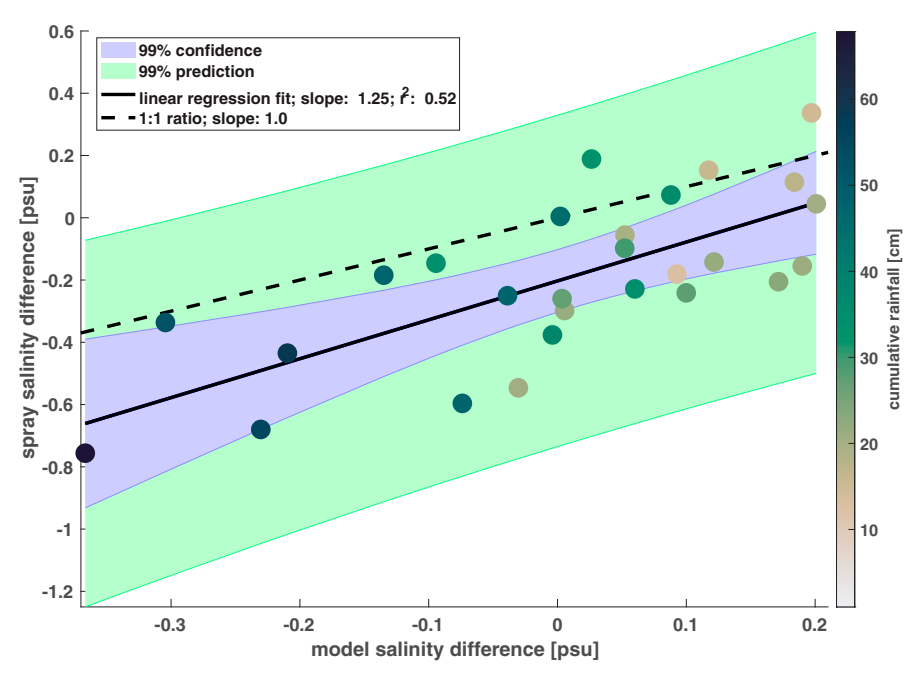


FIG. 2. Observed vs modeled March-minus-September salinity differences (psu) color coded by cumulative rainfall (cm) for the years 2008–19. The solid black line represents the linear regression of observed to modeled salinity data for all rain rates, plotted with 99% confidence (blue shading) and prediction (green shading) intervals. The slope and r^2 value for the fit are indicated in the legend. The black dotted line indicates the 1:1 relationship. Data are included from coastal, onshore, and offshore locations. With 27 data points, linear regression coefficients are statistically different from zero at the 99% confidence level if $r^2 > 0.24$; our results exceed this threshold.

To isolate the impact of wind speed on surface mixing, values for radiation (I_L and I_S), specific humidity (SpH), and air temperature T_a are kept constant and set as the calculated average value of the ERA5 dataset over five coastal AR events from October 2016 to February 2017. Characteristic precipitation, wind speed, and event duration are defined based on commonly occurring conditions for AR events, as noted in the statistical distribution of different conditions for composited AR events from Table 2 in Ralph et al. (2013). Precipitation is applied as a 12-h-long Gaussian pulse (defined by the full width of the Gaussian at one tenth of the peak) with maximum rain rate (R = 0, 2, 3, 4, 5,and 8 mm h⁻¹) occurring during the 48th hour, preceded and followed by a period of zero rainfall. The Gaussian pulse was chosen based on work of Drushka et al. (2016), who showed that for the same cumulative rainfall, the maximum rain rate was more important than pulse width in determining the salinity response. Wind speed is applied as a constant value ($U = 0, 2, 4, 8, 12, 16 \text{ m s}^{-1}$) over the 4-day time period. The six different rain conditions and six different wind conditions result in a total of 36 model runs. Figure S1 in the online supplemental material shows an example of idealized forcing and modeled ocean response for one sensitivity run. The model parameters for this study are also listed in Table 1.

For event-focused simulations, the initial temperature profile is set as the interpolated profile averaged over five coastal

AR events from October 2016 to February 2017 from Spray glider data on line 66.7. The initial salinity profile is constant with depth to allow the vertical change in salinity from precipitation to be distinguished from mixing. The salinity at all depths is set to the 10-m salinity from Spray averaged over the same five coastal AR events. The decision to adopt a constant vertical salinity profile is justified by the results of sensitivity tests that indicate that variations in the stratification of the initial vertical salinity profile have little effect on the salinity response to rain events (not shown). In contrast, in a different regime in the tropics, Drushka et al. (2016) and Iver and Drushka (2021) find that rain falling on saltier water will lead to a larger salinity stratification than rain falling on freshwater, and that the preexisting background salinity can have a larger impact on the salinity response to rain than the rain conditions themselves.

Following Drushka et al. (2016), two metrics are defined in order to characterize the ocean response to rainfall: the depth (D_L) and duration (T_L) of the fresh lens. Here the fresh-lens depth D_L is defined as the depth at which the salinity anomaly relative to the salinity at the first time step is 25% of the maximum anomaly. In contrast Drushka et al. (2016) defined D_L where the salinity anomaly relative to a no-rain control run was 10% of the maximum anomaly. The lifetime of the fresh lens T_L is defined as the time period over which the fresh-lens depth is nonzero. The definition of D_L differs from that of Drushka et al. (2016) in order to account for AR conditions

in the CCS, as ARs in the CCS have smaller rain rates but longer duration than rain events in the tropics. To compare the model simulations for different external forcing cases, we calculate the salinity difference ΔS as the salinity at 0.01-m depth at each time step subtracted from the 0.01-m depth salinity at the first time step. A positive ΔS therefore represents a decrease in surface salinity over time. The maximum vertical salinity difference $\Delta S_{\rm max}$ is defined as the maximum value of ΔS within the 4-day time period.

3) MODEL SETUP, CASE STUDIES

Event case studies are run using the one-dimensional configuration of the MITgcm to study the impact of specific AR events on the formation of freshwater lenses. The event length is set to nine days to match the MBARI composite studies. Five different coastal AR events are chosen: (i) 16 October 2016, (ii) 27 November 2016, (iii) 11 December 2016, (iv) 19 January 2017, and (v) 17 February 2017. Atmospheric forcing is applied hourly and is linearly interpolated to 60 s time steps by the model. Values for rain rate (R), wind speed $(U_Z \text{ and } U_M)$, radiation $(I_L \text{ and } I_S)$, specific humidity (SpH), and air temperature (T_a) are taken from the ERA5 dataset at the coastal location for a duration starting 3 days before and ending 6 days after the event date. Figure S2 in the online supplemental material shows an example of the forcing for one of the five runs. The initial temperature and salinity profiles are set as the profile for each event starting date from the Spray glider at the coastal location along line 66.7, interpolated to telescoping depths. As in the sensitivity studies, ΔS_{max} is calculated for each model run as the maximum value of the difference in salinity at 0.01-m depth between each time step within the 9-day time period and the first time step. Model output from case studies is compared to that of the sensitivity studies, as well as observational results from the MBARI M1 mooring. The model parameters for this study are also listed in Table 1.

4) MODEL VALIDATION

A one-dimensional model (the MITgcm ocean column; Adcroft et al. 2018) will allow for analysis without impacts from horizontal advection or runoff. To validate the use of the MITgcm for event-based studies, we first run with external forcing and initial conditions used by Drushka et al. (2016) for a site in the tropical Pacific and compare with the published results of the General Ocean Turbulence Model (GOTM) by Drushka et al. (2016). For consistency with GOTM outputs, in this model validation ΔS_{max} is defined as the maximum vertical salinity difference between 5 m and 0.01 m, following Drushka et al. (2016). MITgcm results are similar to GOTM results (Fig. S3). One difference is that the MITgcm KPP tends to mix deeper and preserves the freshwater lens for a shorter duration, except in the case of 10 m s⁻¹ winds and 2 mm h⁻¹ precipitation rates (not shown). As a result, the maximum vertical salinity difference between 5 and 0.01 m for a given model run is generally smaller in the MITgcm than in GOTM. Conversely, at higher rain rates, GOTM has greater mixing of large

freshwater inputs at the surface, resulting in a lower maximum vertical salinity difference than in MITgcm for 2 m s⁻¹ (not shown) winds and 50 mm h⁻¹ precipitation rates. However, for most rain and wind cases a statistically significant 1:1 linear fit is exhibited between the two models (Fig. S3). Therefore, differences between GOTM and the MITgcm are judged minor. Since the MITgcm is consistent with the one-dimensional turbulence model, we choose to use it here because it can later be extended to run in a three-dimensional configuration, which will aid in future work considering ocean processes such as horizontal advection, runoff, and upwelling.

Sensitivity experiments are run to test other parameters of the MITgcm, including the model time step, the KPP Richardson number threshold for mixing, and the initial stratification (not shown). Model results are relatively insensitive to time step and only sensitive to Richardson number threshold at high rain rates in combination with low wind speeds. Initial stratification is tested by changing the input vertical salinity profile to have different slopes within a salinity range of 33–34 psu in the upper 20–80 m of the water column (not shown). These changes are found to have little impact on the vertical changes in salinity in response to different rain rates.

5. Results

a. Seasonal response

While changes in the salinity of the CCS have previously been attributed mainly to advection (Lynn and Simpson 1987; Schneider et al. 2005), the time series for the MBARI M1 Mooring salinity and the MITgcm model output salinity at 1-m depth in comparison to ERA5 daily cumulative precipitation both suggest that local precipitation also impacts ocean surface salinity (Fig. 3). A seasonal freshening is present from September to March for the years 2015-18 in both mooring and model data, with the exception of 2017 for the mooring (Fig. 3). Here, the mooring data often show the freshening to be a response to rain events, as typically spikes in precipitation (10-35 mm day⁻¹) are followed by decreases in salinity (0.1-1.0 psu). The comparison of model and mooring salinities in Fig. 3 shows that the mooring has a more drastic salinity response immediately following rain events, while the model response is more gradual (up to 0.25 psu). While Fig. 3 suggests a relationship between seasonal precipitation and salinity change, its inclusion here is mainly intended as an introduction to the idea that salinity changes in the upper ocean may be linked to precipitation. Data from the MBARI M1 mooring are further analyzed in sections 5b(1) and 5b(3).

We also examine annual and interannual variability of salinity as measured by the Spray glider and precipitation from ERA5 (Fig. 4). The annual climatological salinity anomaly in Fig. 4a shows that at all locations there is a negative salinity anomaly (blue) during the rainy season months of October–April. A positive anomaly (red) is seen during the summer months May–September. This pattern is stronger

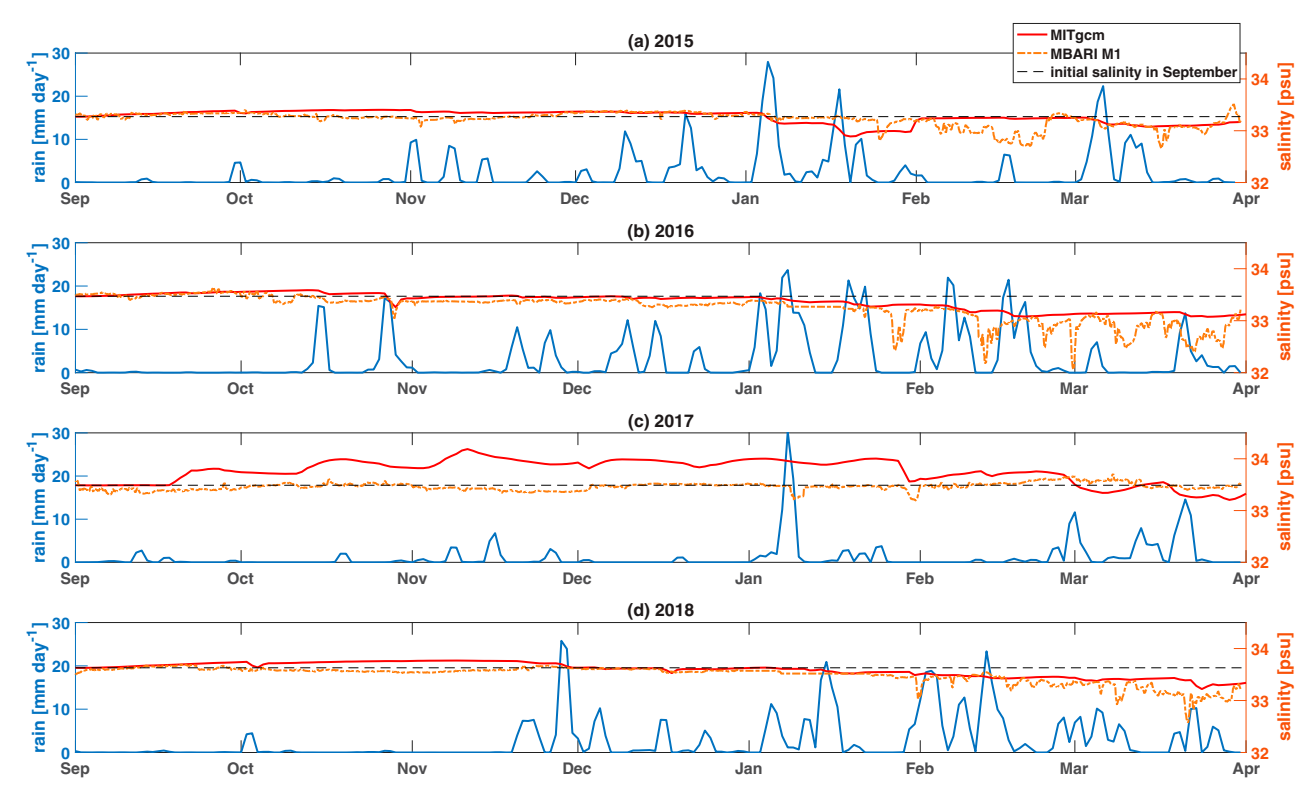


FIG. 3. Time series showing salinity (psu) for MITgcm one-dimensional model runs (red, solid) and MBARI M1 mooring (red, dashed) at 1-m depth, compared to ERA5 rain rate (mm day⁻¹) (blue) from September through March in (a)–(d) 2015–18. The black dashed line represents the initial salinity in September for comparison.

at the coast than offshore. The annual cycle of negative anomaly in the winter (October-April) and positive anomaly in summer (May-September) is also often visible in the full time series (Figs. 4b,d). For example, high precipitation in the 2016/17 rainy season (Fig. 4d) coincides with a negative salinity anomaly (Fig. 4d and blue in Fig. 4b), while lower precipitation in the 2017/18 season coincides with a positive, or less negative, salinity anomaly (Fig. 4d and red in Fig. 4b). Figure 4e shows that the salinity anomaly averaged over the top 40 to top 150 m is rather insensitive to the depth range over which it is averaged (red lines), suggesting that processes other than local rain (e.g., runoff, advection) play a role in these salinity changes. However, the all-rain scenario is used here as a limiting case by applying these salinity anomalies in Eq. (1) to calculate the amount of precipitation that would theoretically produce the anomaly if evaporation and rain were the only contributing factors (blue line, Fig. 4e). This information is then used to compute the ratio of observed cumulative local precipitation from September to January of each year to the theoretical cumulative precipitation that could account for the annual cycle of freshening. Here, Fig. 4f shows that ratio and indicates that local rain could potentially account for up to 100% of the annual cycle of freshening in the upper 50 m in this limiting case in which the system depends only on vertical mixing, with no effect due to horizontal advection. The precipitation required to produce the annual salinity anomaly over the depth range increases

with increasing depth, which leads to estimated rain fraction decreasing with increasing integration depth. In other words, as we integrate to greater depth, a smaller portion of the salinity signal is expected to be due to rain. Determining the mechanisms responsible for the residual, which possibly include horizontal advection, runoff, upwelling, or downwelling, is outside the scope of this study.

To characterize upper-ocean freshening in response to precipitation, for both glider and model data, we plot the March-minus-September salinity differences at 10-m depth as a function of cumulative rainfall at coastal, onshore, and offshore locations (Figs. 5a-c). We also include salinity differences as measured from the MBARI M1 mooring at the coastal location. The quantities appear anticorrelated: high cumulative rainfall typically corresponds to larger salinity decreases (Figs. 5a-c). For glider, mooring, and model data, least squares fits show negative slopes and r^2 values that are statistically significant at the 95% level (corresponding to $r^2 > 0.30$ for 12 years of data), except at the offshore location. These r^2 values suggest that precipitation can explain a significant portion of the variance in the surface salinity difference over the rainy season at coastal and onshore locations (52% and 59% for the glider data, 50% for the mooring data, and 84% and 62% for the model output). The offshore region does not always show a salinity decrease over the course of the water year, and it also tends to experience a lower cumulative rainfall than coastal and onshore

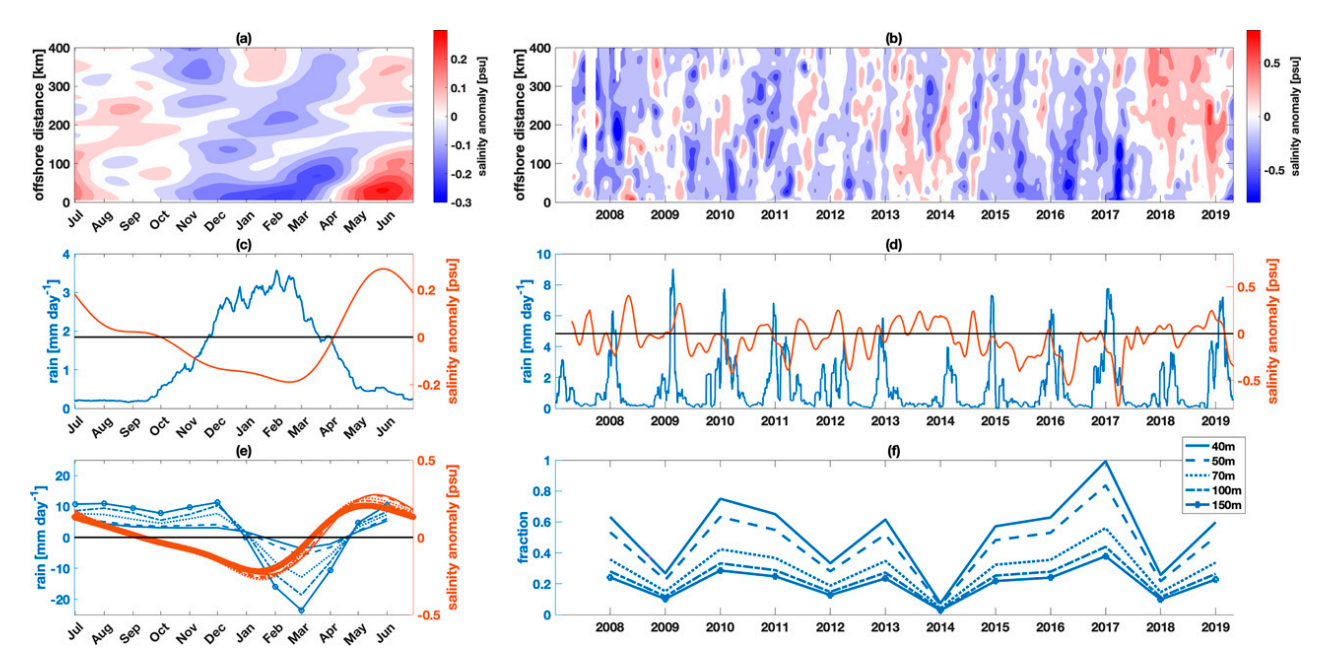


FIG. 4. (a) Climatological annual cycle and (b) multiyear time series of salinity anomaly as a function of offshore distance at 10 m depth as measured by the CUGN Spray underwater glider on line 66.7. (c),(d) Salinity anomaly averaged over offshore distances from 0 to 50 km (red) and daily precipitation with a 30-day moving mean at the coastal location (blue; offshore distance < 50 km): annual signal averaged over 2007–19 in (c) and time series in (d), showing interannual anomaly for salinity and a 30-day moving mean for daily precipitation. (e) Salinity anomaly averaged over different depths (40, 50, 70, 100, and 150 m) in the upper ocean at 15 km offshore (red) and theoretical daily precipitation that would be required if local rain was the only factor leading to a change in salinity (blue). (f) Ratio of observed cumulative precipitation from September to January of each year to cumulative precipitation that would be required to produce the annual salinity anomaly in (e) for different depths. Spray data from Rudnick et al. (2017a); evaporation and precipitation data from ERA5.

locations (15–45 cm for offshore in comparison to 20–70 cm for coastal). The model response differs from the observational data in that the model tends to show a smaller decrease in salinity over the season (Figs. 5a–c), as discussed in section 4a(3).

Given the one-dimensional nature of the model, external forcing would be expected to explain 100% of the variance in salinity changes, which is not the case in Fig. 5. Here, unexplained variance results from not including evaporation and analyzing salinity changes only at the surface, thus not capturing mixing of the freshwater input to further depths. When comparing evaporation minus precipitation to the salinity change integrated over all depths, 100% of the variance is explained by the model for all locations (not shown).

To further investigate the role that ARs play in seasonal upper-ocean freshening, we compare the number of AR events to the March-minus-September 10-m salinity difference for glider data at the three locations (Figs. 5d–f). Years with more ARs tend to exhibit larger salinity decreases, as seen in Figs. 5d–f and as indicated by the negative slopes of the regressions. This is the case except in 2017 at the offshore location, when an increase in salinity is seen despite a large number of ARs (Fig. 5d). Similarly to the relationship between cumulative rainfall and salinity difference, this trend is statistically significant at the 95% level, except at offshore locations, and r^2 values suggest that ARs can explain a significant portion of the variance in salinity

difference over the rainy season for coastal and onshore locations. At offshore locations, relationships between the number of AR events and salinity difference (Fig. 5d) or precipitation and salinity difference (Fig. 5a) do not exhibit r^2 values for linear regression that are statistically significant. The lack of correlation between local rainfall and freshening at offshore locations could be caused by salinity changes related to processes other than rainfall, such as advection.

b. Event-based response

1) EVENT COMPOSITES

While the results of section 5a demonstrate that in the CCS region, the upper ocean freshens more during high rainfall years than it does in low rainfall years, the question of whether individual rainfall events are detectable in upper-ocean salinity remains. We begin examination of the ocean salinity response to rain events on short time scales by using event composites. Figure 6 shows a time series composited from 85 events that occurred at the MBARI M1 mooring location from January 2007 to March 2019 (see Fig. S4). The rain events that are in the composite analysis are shown as both cumulative rain over 6 h (red) and daily cumulative precipitation (blue), whereas salinity is plotted as a 6-hourly moving mean. In Fig. 6, relative day zero represents the first day that rainfall exceeded a threshold of 5 mm day⁻¹

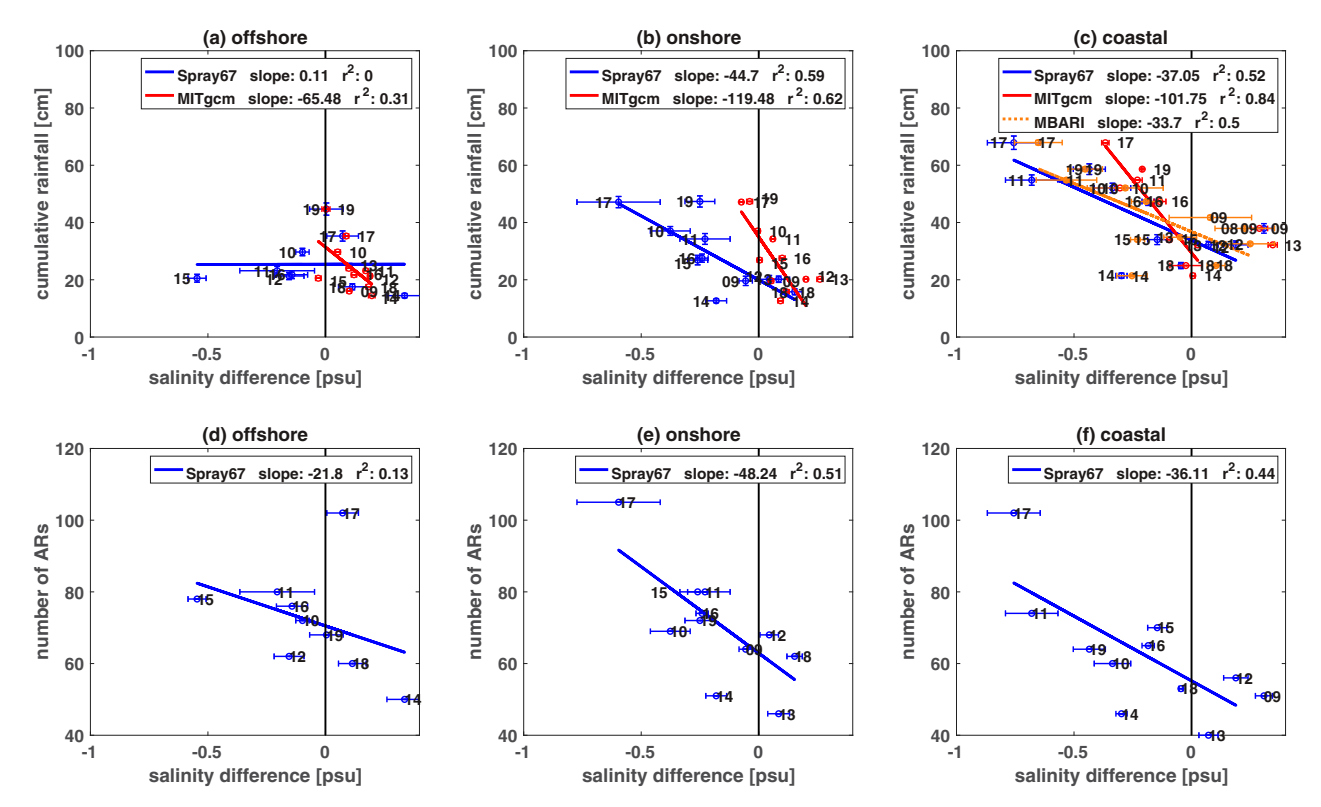


FIG. 5. (top) Cumulative rainfall (cm) and (bottom) number of AR events as a function of salinity (psu) difference between March and September for the years 2008–19 at (a),(d) offshore, (b),(e) onshore, and (c),(f) coastal locations. Panels (a)–(c) include CUGN Spray line 66.7 observations (blue), MBARI M1 mooring observations (red, dotted), and MITgcm one-dimensional model runs (red, solid) at 10 m depth. The blue and red lines represent least squares fits to glider, mooring, and model data with the slope and r^2 values labeled in the legend. Panels (d)–(f) show data from SIO-R1 AR catalog and CUGN Spray line 66.7 observations (blue) at 10-m depth. Blue lines represent linear regressions, with slopes and r^2 indicated in the legends.

[a result of the event compositing discussed in section 4b(1)]. The wind speed (Fig. 6b) remains relatively constant at about 5 ± 1 m s⁻¹ for the duration of the composite time series, with a slight peak on relative days 0–1. Figure 6c shows that the surface salinity measured by the M1 mooring decreases over the duration of the composite time series, especially during the days with peak rain (day 0 through 1). While there is an increase in salinity from day 1 through day 4, overall the salinity is lower at the end of the composite time series than at the beginning. The results from this composite study indicate that salinity measurably decreases in response to rain on an event basis. To assess the mechanisms governing this freshening pattern, we use the model to carry out event sensitivity studies.

2) MODEL SENSITIVITY STUDIES OF RAIN AND WIND EFFECTS IN FRESHWATER LENS FORMATION

Event-based studies are performed using the one-dimensional MITgcm configured for the CCS. The model allows us to isolate the impacts of rain and wind on upper-ocean salinity stratification and to determine whether the resulting vertical salinity change will be detectable, given the 0.01-psu resolution of CTD instruments (as discussed in section 3a). While the range of salinity responses depends on rain rate and wind speed on event time scales, this study highlights two key mechanisms

that govern salinity changes as a function of precipitation and wind speed: (i) mixing of the freshwater or (ii) development of freshwater lenses at the surface.

Figure 7 shows the salinity anomaly in the upper ocean in response to a range of model input conditions (wind speeds increase from 2 to 16 m s⁻¹ from top to bottom, and rain rates increase from 2 to 8 mm h⁻¹ from left to right), normalized to the maximum salinity anomaly for each given wind speed and rain rate. Two extreme cases are detected: (i) vertical mixing of the freshwater to depths greater than 20 m at high wind speeds ($U > 8 \text{ m s}^{-1}$) and (ii) development of freshwater lenses at the surface for low wind speeds ($U \le 8 \text{ m s}^{-1}$), where the depth of the fresh lens is depicted by the black lines of Fig. 7. This is consistent with results from Thompson et al. (2019), where stable rain layers were found to persist with wind speeds up to 9.8 m s⁻¹. As wind speed increases (moving top to bottom) the freshwater lens is brought to a greater depth and remains over a shorter time period than at low wind speeds, except in the case of $R = 2 \text{ mm h}^{-1}$ where the small freshwater input may impact the trend in lens depth. As rain rate increases (moving left to right) the freshwater input is mixed over a deeper range, except in the case of $U = 2 \text{ m s}^{-1}$; additionally, the lens has a longer duration with increasing rain rate. These results are reproduced in Fig. 8.

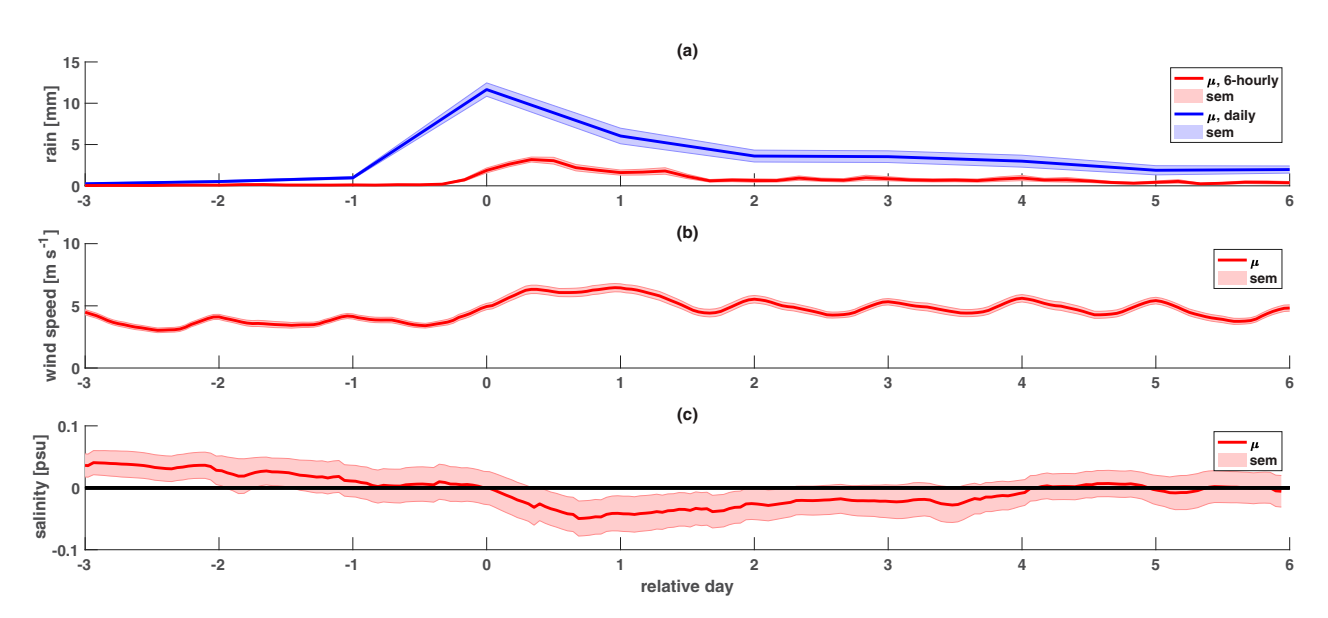


FIG. 6. Composite time series of (a) 6-hourly rain (mm; red) and daily cumulative rain from day -3 to day n (mm; blue), (b) wind speed (m s⁻¹) with a 6-h moving mean, and (c) salinity difference (psu) between relative day n and relative day 0 for 85 rain events occurring at the MBARI M1 mooring location from January 2007 to March 2019. The solid line (μ) represents the mean of all composite events and the shading represents the standard error of the mean (sem) among these events. The solid black line in (c) represents a salinity of zero, which is zero on day zero because the anomaly is in reference to this day. Events are included if daily cumulative precipitation on day zero is greater than 5 mm day⁻¹ and there has not been another rain event within 10 days of the event start date. Event start dates are set as the first date that rainfall exceeds the threshold; conditions are shown from 3 days before through 6 days after this date. Rainfall and wind speed are taken from ERA5 and salinity from the MBARI M1 mooring.

The dependence of the vertical salinity gradient on rain and wind speed is shown in Fig. 8. In Figs. 8a and 8b, the maximum vertical salinity difference ΔS_{max} [defined in section 4b(2)] increases as a function of rain rate and decreases as a function of wind speed. Modeled freshwater lens depth (D_L) and duration (T_L) are shown as a function of wind speed and rain rate in Figs. 8c and 8d. Here, an increased wind speed corresponds to deeper mixing, bringing freshwater to a greater depth, therefore decreasing stratification and decreasing the magnitude of ΔS_{max} . At low wind speeds there is minimal mixing, and changes in salinity are confined to the surface (<20 m) and are not prominent at depth, leading to a larger ΔS_{max} (Figs. 8a,b). In this case, a freshwater lens is formed at the surface, and stratification is enhanced. Figures 8a and 8b (reproduced in Fig. 9) also show model output from five event case studies (the colored circles), which fall within the same range for ΔS_{max} as the output from the sensitivity studies with similar rain rates and wind speeds. The black dotted line in Fig. 9 represents the salinity change that is detectable by CTD instruments (0.01 psu). Almost all of the events in the sensitivity studies exceed this threshold, with the only exception being for a rain rate of 2 mm h^{-1} in combination with a wind speed of 16 m s^{-1} .

The results show a relationship between wind, rainfall, and salinity similar to that suggested by Drushka et al. (2016): $\Delta S_{\text{max}} = A R_{\text{max}} U^b$, where constants A and b are solved for using model outputs. Here, rain rates of 0 mm h⁻¹ and wind speeds of 0 m s⁻¹ are omitted from the regression because the fit is representative of cases where rain and wind are present.

For the MITgcm model runs, $A = 0.32 \pm 0.05$ psu (mm h⁻¹)⁻¹ and $b = 1.44 \pm 0.06$. Uncertainties of linear regression parameters are calculated using Monte Carlo methods (Fig. S5). The values of the regression parameters are within five standard deviations of values found by Drushka et al. (2016): $A = 0.11 \pm 0.03$ and $b = 1.1 \pm 0.03$. The values of these coefficients are also similarly related to those found in studies done without the wind dependence both by Drucker and Riser (2014), who found a value A = 0.14 psu (mm h⁻¹)⁻¹ averaged over the tropics, and by Boutin et al. (2014), who found region-dependent values of A that ranged from 0.14 to 0.22 psu (mm h⁻¹)⁻¹ at moderate wind speeds. Differences in these coefficients likely arise as a result of the difference in duration of the applied rain pulse (12 h here for AR studies in CCS versus 1 h for studies in the tropics). While this relationship has been applied in the tropics for the references listed above, we find it does well in representing AR events in the CCS, with an r^2 of 0.97 (Fig. S5). It should be noted that this equation is appropriate for one-dimensional models that do not include advection and may not work well in cases where advection is significant. However, case studies in the following section [section 5b(3)] show this equation does well in representing the magnitude of the salinity response to AR events in comparison to in situ measurements (Figs. 9 and 10).

Freshwater lenses reach depths of 5–50 m, depending on rain rate and wind speed (Fig. 8c). The depth of the fresh lens increases with wind speed for all rain rates, except in the cases of 2 and 3 mm h⁻¹ rain rates where wind is greater than 8 m s⁻¹. These exceptions likely occur because the

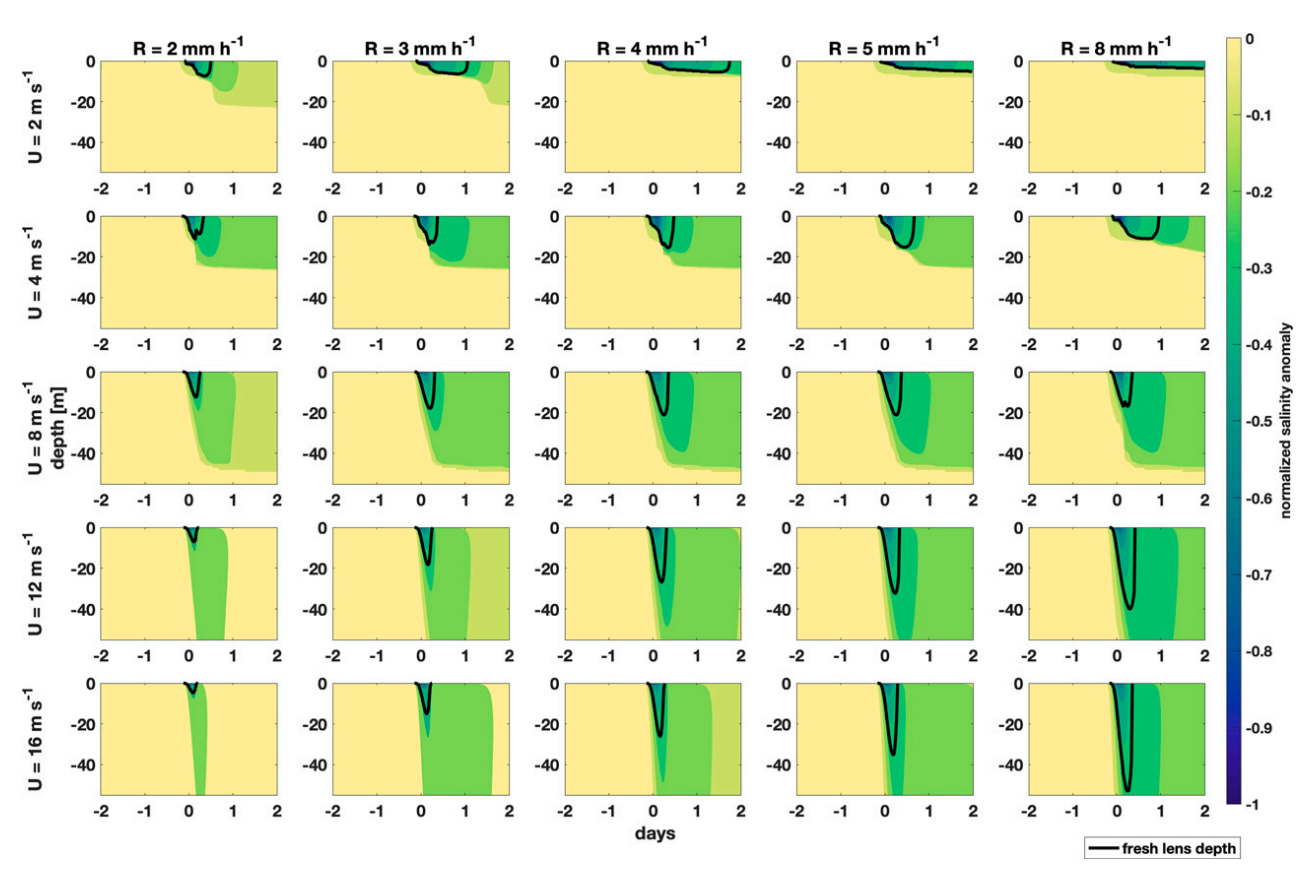


FIG. 7. Normalized salinity anomaly in the upper 55 m of the ocean for the 4-day one-dimensional MITgcm runs and for wind speeds from 2 to 16 m s⁻¹ and maximum rain rates from 2 to 8 mm h⁻¹. Each contour plot is divided by the absolute value of the maximum salinity anomaly for the given rain rate and wind speed. Black lines represent the freshwater lens depth D_L (m), defined as the depth at which the salinity anomaly relative to the salinity during the first time step for each run is 25% of the maximum anomaly.

freshwater input is too small to cause salinity changes at increasing depths during mixing. Additionally, the fresh lens depth increases with higher rain rates, as indicated by the ordering of the colored lines, with the lowest rain rate (light green, 2 mm h^{-1}) having the smallest D_L and the highest rain rate (dark blue, 8 mm h^{-1}) the largest D_L . This is true except in the cases of low wind speed and high rain rate $(U = 2, 4, \text{ and } 8 \text{ m s}^{-1} \text{ and } R = 8 \text{ mm h}^{-1})$, where the magnitude of the salinity response is comparatively large ($\Delta S_{\text{max}} = 1.3, 0.55$, and 0.2 psu). These events fall outside the trend for D_L because for each particular combination of wind speed and rain rate these metrics are defined based on the maximum salinity anomaly relative to the salinity at the first time step, which for these extreme cases is much higher than the average salinity anomaly for a particular rain rate or wind speed. Freshwater lenses last anywhere from 10 to 50 h, depending on rain rate and wind speed (Fig. 8d). The duration of the freshwater lens T_L shows a pattern of decreasing with increasing wind speed and decreasing rain rate. For wind speeds greater than 8 m s⁻¹ the lens duration has a much smaller range of 10-15 h.

Results for the fresh lens depth, D_L , are in agreement with the 20-m mean stable layer depth in central Indian Ocean found by Thompson et al. (2019). These results also show similar trends to the tropical results of Drushka et al. (2016). One

difference is that for these studies of characteristic AR events in the CCS, the depth and duration of the freshwater lens are much larger than studies done in the tropics. This is likely a result of the fact that AR events in the CCS have a much longer rainfall duration than rain events in the tropics (12 versus 1 h). This is confirmed by runs done in the CCS with 24-h rain pulses (not shown), where D_L and T_L increased even more from the 12-h rain pulse case. It should be noted that D_L and T_L are highly sensitive to the lens definition, as discussed in section 4b(2). Decreasing the percentage of the maximum salinity anomaly that defines the depth leads to overall increases in D_L and T_L . This makes sense because a less drastic salinity anomaly is expected to reach greater depths for a longer duration. As an example of this sensitivity, for a rain rate of 8 mm h⁻¹ and U = 12 m s⁻¹, when D_L is defined as the depth at which the salinity anomaly is 15% of the maximum anomaly, rather than 25%, it reaches a maximum of 80 m instead of 53 m. Correspondingly, the time T_L reaches a maximum of 95 h instead of 50 h.

3) MODEL CASE STUDIES

Event case studies are performed using the one-dimensional MITgcm configured for the CCS at the start of each of five different AR events (Table 1). The model allows us to isolate the

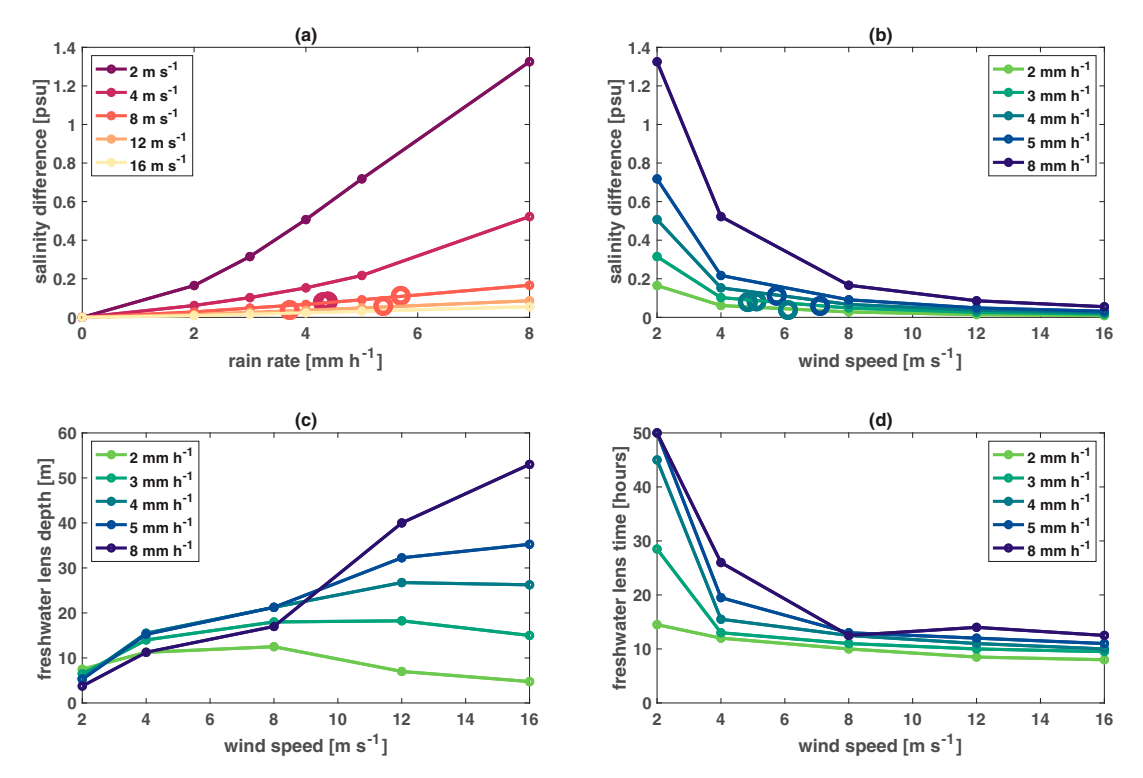


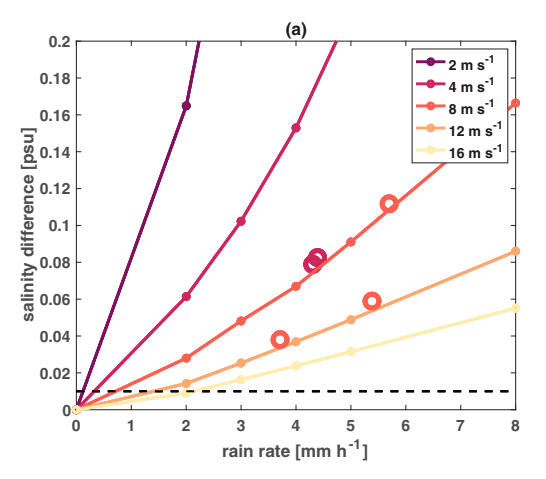
FIG. 8. Results from the MITgcm experiments using idealized environmental forcing in which the peak rain rate and the wind speed are varied. (a) Peak magnitude of ΔS , $\Delta S_{\rm max}$, as a function of rain rate for five different wind speeds; (b) $\Delta S_{\rm max}$ as a function of wind speed for different rain rates; and maximum (c) thickness D_L and (d) lifetime T_L of the fresh lens as a function of wind speed at different rain rates. The $\Delta S_{\rm max}$ is defined as the maximum value of the salinity difference at 0.01-m depth from the salinity at the first time step within the 4-day simulation time period. In both (a) and (b), the colored circles show model output from event case studies, with the colors representing wind speed and rain rate, respectively.

impacts of atmospheric forcing on upper-ocean salinity stratification and to determine whether the resulting vertical salinity change may be detectable, given the 0.01-psu resolution of CTD instruments (as discussed in section 3a). The results from three case studies are shown in Fig. 10, where the different columns (i.e., Figs. 10a,d; Figs. 10b,e; Figs. 10c,f) represent each of the three different events. Figures 10a-c show the rain rate (blue) and wind speed (red) from ERA5 at the coastal location that was used as forcing for the model. Figures 10d-f show the response of salinity difference (ΔS) from the first time step at 0.01-m depth for the model (red, solid) and 1-m depth for the MBARI M1 mooring (orange, dotted). The magnitude of the model and mooring ΔS responses are similar, while their temporal structure is not. The mooring often has a slower response that lasts a longer duration. These differences are likely due to the fact that the model is one-dimensional and solely shows a salinity response to rain, while the mooring captures runoff and advection of waters from other locations that were impacted by the rain events, and thus changes continue to occur once the local rain has stopped. Here, the black dotted line indicates ΔS values that are detectable by CTD instruments (0.01 psu), showing that all three AR events produced measurable changes in salinity. Additionally, Fig. 9 shows the results from five modeled case studies overlaid on results from the model sensitivity

studies (colored circles), as a function of both rain rate and wind speed. The black dotted line indicates ΔS values that are detectable by CTD instruments (0.01 psu). All of the case studies shown produce salinity changes greater than the measurable threshold. The ΔS values for the case studies fall within the range of the sensitivity studies for a given rain rate and wind speed, as discussed in section 5b(2). Overall, the salinity difference ΔS in the modeled case studies is consistent with outputs from the model sensitivity studies for characteristic AR events, as well as with observations at the MBARI M1 mooring.

6. Discussion

The purpose of this study has been to evaluate the impact of atmospheric forcing on surface ocean salinity in the CCS. A one-dimensional ocean model can help isolate the salinity response to rainfall events in comparison to other intrinsic ocean dynamics. While changes in salinity in the CCS have previously been largely attributed to southward horizontal advection of low-salinity water from the northeast Pacific (Lynn and Simpson 1987; Schneider et al. 2005), this analysis has shown that the salinity changes could also be attributed to freshwater inputs in the form of precipitation from atmospheric rivers on both seasonal and event time scales.



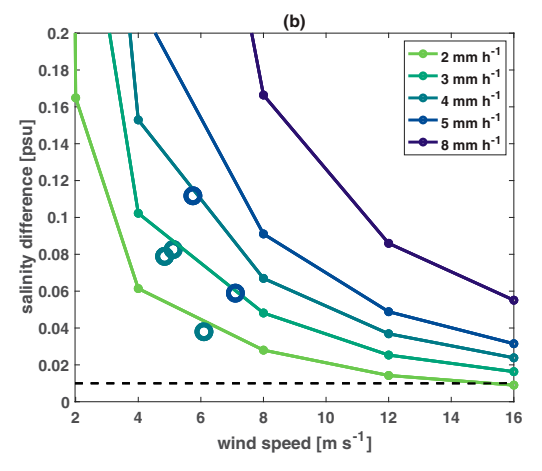


FIG. 9. As in Figs. 8a and 8b, but zoomed in to enhance view of results from event case studies (colored circles). The colored circles show model output from event case studies, with the colors representing wind speed and rain rate, respectively. The black dotted line represents the salinity difference of 0.01 psu that is detectable by CTD instruments.

a. Seasonal response

Seasonal freshening in the CCS depends on cumulative rainfall. Results in section 5a compare ERA5 rainfall to salinity from observational data (mooring and underwater glider) and one-dimensional model output. While intrinsic ocean processes should be captured by observations, most are not represented by the one-dimensional model. Despite this omission, the model nonetheless shows a statistical relationship between cumulative rainfall and salinity difference (Fig. 5). These analyses support the idea that local rainfall may be one of several mechanisms playing a role in the seasonal salinity response, and that it is a significant enough component to account for anomalously fresh or salty years.

We find that there is a stronger salinity signal in coastal locations for both observations and model outputs. As discussed in section 5a, this could be attributed to the fact that there is a higher cumulative rainfall at coastal locations. Additionally, processes omitted by the model, including upwelling, runoff, and advection, could all play a role in the observational results. For example, Auad et al. (2011) suggest that upwelling of cool, saline water enhances coastal salinity increases in the summer, which could contribute to a larger positive salinity anomaly in summer (September) and a larger difference in March minus September salinity. Freshwater input from riverine runoff has also been linked to decreases in surface salinity measurements. AR precipitation events occur more often on land than over the ocean (Fig. 1a), which might lead to runoff. Riverine input from the Salinas River that discharges into Monterey Bay has been linked to decreases in surface salinity as measured by the MBARI M1 mooring (Kudela and Chavez 2004). River discharge from the Sacramento/San Joaquin River system 100 km north of the M1 mooring has also been linked to low-salinity measurements off the coast of Monterey Bay (Johnson et al. 1999).

Southward advection of freshwater in the low-salinity tongue of the California Current has been previously described as the main source of salinity changes in the CCS

(Auad et al. 2011; Lynn and Simpson 1987; Schneider et al. 2005). While we do not find evidence against this, when looking at the seasonal cycle of CCS advection there are a few instances of anomalous salinity that may not be linked to advection. For example, the low surface salinity anomaly seen 50 m offshore along CalCOFI line 66.7 during the winter months (Fig. 4.2.3.1 in Rudnick et al. 2017b) is unexplained by the strong poleward current at this location and time which would be expected to carry saltier water from further south. On longer time scales (5–10 years), Schneider et al. (2005) found that negative anomalies in salinity storage averaged over the top 150 m corresponded to increased precipitation, but also noted that patterns in salinity anomaly imply freshwater fluxes that are larger than the observed precipitation or evaporation anomalies. This is supported by Fig. 4f, which shows that the observed precipitation is 3%-30% of the precipitation that would be required to produce the salinity anomaly in the upper 150 m if all other terms in the salinity balance are ignored. While this may be the case for the salinity changes in the upper 150 m, we have shown the observed precipitation can explain up to 100% of the seasonal salinity change in the upper 40 m.

While some of the salinity changes may be linked to runoff, upwelling, or advection, the one-dimensional nature of the model omits these ocean dynamics that might have a visible impact on mooring and glider data. Nonetheless, the model still shows a seasonal salinity response to freshwater inputs from rain, as discussed in section 5a.

b. Event-based response

On event time scales, certain combinations of rain rate and wind speed can lead to the formation of freshwater lenses. Freshwater lenses may inhibit mixing of surface waters and increase upper-ocean stratification, which has a variety of implications for the exchange of heat and moisture between the ocean and atmosphere, as discussed in section 2d (SPURS-2 Planning Group 2015; Williams et al. 2006). Understanding the structure

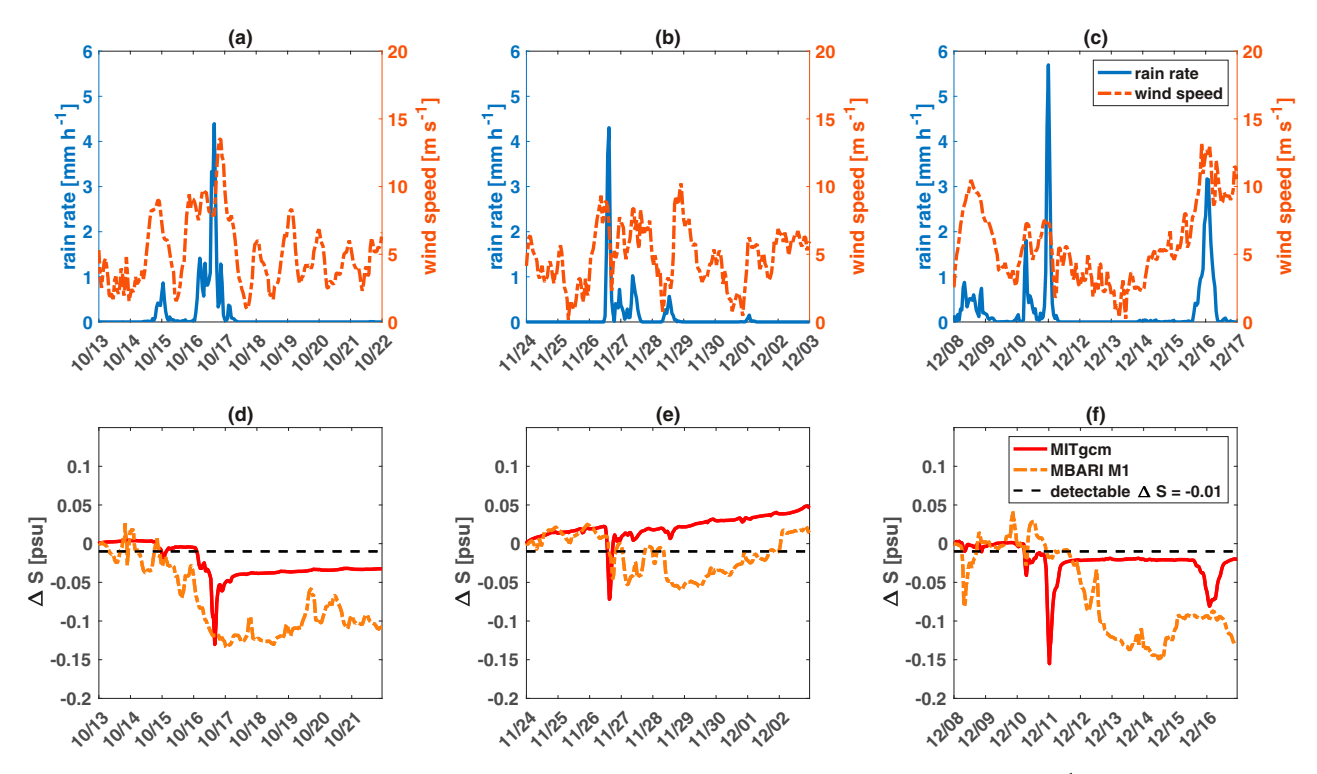


FIG. 10. Results from case studies for three AR events in the CCS. (a)–(c) Time series of rain rate (mm h⁻¹; blue) and wind speed (m s⁻¹; red) that was used as model forcing from ERA5 at the coastal location; (d)–(f) time series showing the salinity difference (ΔS ; psu) from the first time step at 0.01-m depth for the model output (red, solid) and at 1-m depth for the MBARI M1 mooring (orange, dotted). The black dotted line in (d)–(f) indicates the salinity difference of 0.01 psu that is detectable by CTD instruments. The start date for event 1 in (a) and (c) is 16 Oct 2016; event 2 in (b) and (e) is 27 Nov 2016; and event 3 in (c) and (f) is 11 Dec 2016. The model runs were initialized 3 days before this date and run until 6 days after.

and evolution of these lenses is important for understanding the possible impacts on air–sea exchanges.

The wind speed and rain rate dependences of ocean surface salinity are investigated using event composites and one-dimensional model sensitivity studies. We show that salinity decreases in response to rain events (section 5b). Furthermore, model results show that the salinity change during a rain event depends linearly on the rain rate and is inversely proportional to wind speed [section 5b(2)]. This suggests that for low wind speeds, freshwater inputs are trapped at the surface and lead to the formation of freshwater lenses, while high wind speeds cause freshwater from rain to mix as deep as 50 m and prevent the formation of long-lasting fresh lenses.

Many events characteristic of ARs in the CCS produce measurable changes in salinity. As discussed in section 5b, there is only one instance where the sensitivity studies do not produce a salinity changed that exceeds the 0.01-psu detectable limit (low rain rate in combination with high wind speed). Additionally, all modeled and observed case studies produce measurable salinity changes. Case studies show that single AR events can produce salinity decreases of up to 0.1 psu that last up to 50 h (Fig. 8). These salinity anomalies are comparable to the decreases in salinity over the entire rainy season, which are shown to be as high as 0.8 psu for observations, and 0.4 psu for one-dimensional models where

effects from advection, runoff, and upwelling are excluded (Fig. 5). It should be noted that while a single AR event may not cause a large, long-lasting drop in salinity, there is a range of salinity change depending on the strength of the given AR. Additionally, ARs often occur in series with several in a row, which may lead to a larger integrated effect over time. Statistics from a composite analysis of 91 AR events from Table 2 of Ralph et al. (2013) indicate that the average maximum rain rate for these events is 4.09 mm h⁻¹ and the average wind speed is 12.8 m s⁻¹. Based on our results, these events would produce salinity changes above the measurable threshold, implying that AR events should be detectable by CTD measurements of ocean salinity.

7. Conclusions

Seasonal freshening in the CCS depends on cumulative rainfall and atmospheric river events, in addition to other intrinsic ocean dynamics that previous studies have identified. At coastal and onshore locations, the CCS freshens throughout the rainy season due to AR events, and years with higher AR activity are associated with a stronger freshening signal (Fig. 5).

Event studies indicate that freshening in the CCS depends on wind speed in addition to rain rate. Low winds lead to conditions that cause freshwater lens formation, while high wind speeds mix freshwater input from rain through the mixed layer. Results from our one-dimensional model show that freshwater lens formation in the CCS is possible in the event of heavy rain and low winds. For events that are characteristic of ARs in the CCS, these lenses are formed often and can last anywhere from 10 to 50 h. The one-dimensional model simulations also suggest that events characteristic of ARs in the CCS tend to produce changes in salinity that are greater than the measurable CTD limit of 0.01 psu, as indicated in Figs. 9 and 10.

Because of the dependence of salinity on both rain and wind, further investigation in the CCS would require local, high-resolution observations of both variables, as was done in the SPURS-2 experiment, in order to develop a more complete understanding. With observations it would also be possible to validate the use of the one-dimensional MITgcm to represent salinity changes on an event time scale, as was done for the seasonal studies [e.g., Fig. 2 in section 4a(3)].

As discussed in section 5b(2), the freshwater lens is highly sensitive to definition. The definitions for D_L and T_L that were shown to work with GOTM for the salinity response to rain events in the tropics (Drushka et al. 2016) were altered slightly for results in the CCS, as discussed in section 4b(2). In another study, Thompson et al. (2019) derived an estimate of the stable layer depth based on wind speed and buoyancy frequency. Future work could explore different forms of the definition specific to the CCS.

While this study has provided evidence that freshwater inputs from rain contribute to variability in ocean surface salinity, the relative importance of horizontal advection, runoff, and external atmospheric forcing has not been addressed. Advection could contribute to the evolution of freshwater lenses by causing increased mixing and by introducing new water into the region. Future studies could address these shortcomings by considering a three-dimensional ocean model that will show the relative importance of horizontal advection and runoff. Additionally, large-scale surface advective salinity transport could be estimated from observations. Future work could also look at the response of properties other than salinity, for example, temperature or biogeochemical properties, and thus elucidate the impact of precipitation events on the climate state.

Acknowledgments. Figures in this report were prepared using MATLAB, Matplotlib: A 2DGraphics Environment (Hunter 2007). DG was supported by NSF Award 1928305. MRM and STG were supported by NASA Awards NNX16AH67G and 80NSSC20K1136. DG and STG were supported by NASA Award 80NSSC19K0059. Authors would like to acknowledge support from CW3E through the California Department of Water Resources funded Atmospheric River Program Phase III (Contract 4600014294). We thank our reviewers for their helpful feedback.

Data availability statement. We acknowledge all sources of publicly available data that were used in this study. This paper contains modified Copernicus Climate Change Service information [2020] in the form of ERA5. The European Commission nor ECMWF is responsible for any use that may be

made of the Copernicus information or data it contains. The ERA5 dataset can be accessed at http://doi.org/10.24381/cds.e2161bac. Data from the CUGN were produced by Daniel Rudnick at Scripps Institution of Oceanography and can be accessed at https://spraydata.ucsd.edu/projects/CUGN/. Mooring data were made available by the Monterey Bay Aquarium Research Institute (MBARI) and can be accessed at https://www.ncei.noaa.gov/archive/accession/0130040. The MITgcm one-dimensional model was made available by the MITgcm contributors (Adcroft et al. 2018). The SIO-R1 Atmospheric River Catalog can be accessed at https://weclima.ucsd.edu/data-products/. All of the data and code used for processing for this paper can be accessed at https://doi.org/10.6075/J0BV7GGW.

REFERENCES

- Adcroft, A., and Coauthors, 2018: MITgcm User Manual. https://doi.org/10.5281/zenodo.1409237.
- Asher, W. E., A. T. Jessup, R. Branch, and D. Clark, 2014: Observations of rain-induced near-surface salinity anomalies. *J. Geophys. Res. Oceans*, 119, 5483–5500, https://doi.org/10.1002/2014JC009954.
- Auad, G., D. Roemmich, and J. Gilson, 2011: The California Current System in relation to the Northeast Pacific Ocean circulation. *Prog. Oceanogr.*, 91, 576–592, https://doi.org/10.1016/j.pocean.2011.09.004.
- Bograd, S. J., T. K. Chereskin, and D. Roemmich, 2001: Transport of mass, heat, salt, and nutrients in the southern California Current System: Annual cycle and interannual variability. J. Geophys. Res., 106, 9255–9275, https://doi.org/10.1029/1999JC000165.
- Boutin, J., N. Martin, G. Reverdin, X. Yin, and F. Gaillard, 2013: Sea surface freshening inferred from SMOS and ARGO salinity: Impact of rain. *Ocean Sci.*, 9, 183–192, https://doi.org/10.5194/os-9-183-2013.
- —, —, S. Morisset, X. Yin, L. Centurioni, and N. Reul, 2014: Sea surface salinity under rain cells: SMOS satellite and in situ drifters observations. *J. Geophys. Res. Oceans*, **119**, 5533–5545, https://doi.org/10.1002/2014JC010070.
- Brainerd, K., and M. Gregg, 1997: Turbulence and stratification on the Tropical Ocean-Global Atmosphere-Coupled Ocean-Atmosphere Response Experiment microstructure pilot cruise. J. Geophys. Res., 102, 10437–10455, https://doi.org/10. 1029/96JC03864.
- Chaudhuri, D., D. Sengupta, E. D'Asaro, and S. Shivaprasad, 2021: Trapping of wind momentum in a salinity-stratified ocean. J. Geophys. Res. Oceans, 126, e2021JC017770, https:// doi.org/10.1029/2021JC017770.
- Chavez, F. P., 2015: In situ, meteorological, physical, and profile data collected by Monterey Bay Aquarium Research Institute at OceanSITES site MBARI from 2004-04-30 to 2021-09-07 (NCEI Accession 0130040). NOAA National Centers for Environmental Information, accessed December 2020, https://www.ncei.noaa.gov/archive/accession/0130040.
- Clayson, C. A., J. B. Edson, A. Paget, R. Graham, and B. Greenwood, 2019: Effects of rainfall on the atmosphere and the ocean during SPURS-2. *Oceanography*, 32, 86–97, https://doi.org/10.5670/oceanog.2019.216.
- Davis, R. E., M. D. Ohman, D. L. Rudkick, J. T. Sherman, and B. Hodges, 2008: Glider surveillance of physics and biology in the southern California Current System. *Limnol. Oceanogr.*, 53, 2151–2168, https://doi.org/10.4319/lo.2008.53.5_part_2.2151.

- de Boyer Montégut, C., J. Mignot, A. Lazar, and S. Cravatte, 2007: Control of salinity on the mixed layer depth in the world ocean: 1. General description. J. Geophys. Res., 112, C06011, https://doi.org/10.1029/2006JC003953.
- Delcroix, T., M. J. McPhaden, A. Dessier, and Y. Gouriou, 2005: Time and space scales for sea surface salinity in the tropical oceans. *Deep-Sea Res. I*, 52, 787–813, https://doi.org/10.1016/j. dsr.2004.11.012.
- Dettinger, M., 2011: Climate change, atmospheric rivers, and floods in California—A multimodel analysis of storm frequency and magnitude changes. *J. Amer. Water Resour. Assoc.*, 47, https://doi.org/10.1111/j.1752-1688.2011.00546.x.
- Drucker, R., and S. C. Riser, 2014: Validation of Aquarius sea surface salinity with Argo: Analysis of error due to depth of measurement and vertical salinity stratification. *J. Geophys. Res. Oceans*, 119, 4626–4637, https://doi.org/10.1002/2014JC010045.
- Drushka, K., W. E. Asher, B. Ward, and K. Walesby, 2016: Understanding the formation and evolution of rain-formed fresh lenses at the ocean surface. *J. Geophys. Res. Oceans*, 121, 2673–2689, https://doi.org/10.1002/2015JC011527.
- —, —, A. T. Jessup, E. J. Thompson, S. Iyer, and D. Clark, 2019: Capturing fresh layers with the surface salinity profiler. *Oceanography*, **32**, 76–85, https://doi.org/10.5670/oceanog. 2019.215.
- Fish, M. A., A. M. Wilson, and M. F. Ralph, 2019: Atmospheric river families: Definition and associated synoptic conditions. *J. Hydrometeor.*, 20, 2091–2108, https://doi.org/10.1175/JHM-D-18-0217.1.
- Gershunov, A., 2017: Catalog of landfalling atmospheric rivers along the western coast of North America. Scripps Institution of Oceanography, accessed December 2020, https://weclima.ucsd.edu/data-products/.
- —, T. Shulgina, F. M. Ralph, D. A. Lavers, and J. J. Rutz, 2017: Accessing the climate-scale variability of atmospheric rivers affecting western North America. *Geophys. Res. Lett.*, 44, 7900–7908, https://doi.org/10.1002/2017GL074175.
- Giglio, D., V. Lyubchich, and S. T. Gille, 2020: Seasonal to interannual variability of upper ocean temperature and salinity: The role of atmospheric rivers. *Ocean Sciences Meeting*, San Diego, CA, Amer. Geophys. Union, AI14A-2255, https://agu. confex.com/agu/osm20/meetingapp.cgi/Paper/655323.
- Guan, B., and D. E. Waliser, 2015: Detection of atmospheric rivers: Evaluation and application of an algorithm for global studies. *J. Geophys. Res. Atmos.*, 120, 12514–12535, https://doi.org/10.1002/2015JD024257.
- Hersbach, H., and Coauthors, 2020: The ERA5 global reanalysis. Quart. J. Roy. Meteor. Soc., 146, 1999–2049, https://doi.org/10. 1002/qj.3803.
- Hunter, J. D., 2007: Matplotlib: A 2D graphics environment. Comput. Sci. Eng., 9, 90–95, https://doi.org/10.1109/MCSE. 2007.55.
- Iyer, S., and K. Drushka, 2021: The influence of preexisting stratification and tropical rain modes on the mixed layer salinity response to rainfall. *J. Geophys. Res. Oceans*, 126, e2021JC017574, https://doi.org/10.1029/2021JC017574.
- Johnson, K., F. Chavez, and G. Friederich, 1999: Continental-shelf sediment as a primary source of iron for coastal phytoplankton. *Nature*, 398, 697–700, https://doi.org/10.1038/19511.
- Kudela, R., and F. Chavez, 2004: The impact of coastal runoff on ocean color during an El Nino year in Central California. *Deep-Sea Res. II*, 51, 1173–1185, https://doi.org/10.1016/ S0967-0645(04)00106-7.

- Large, W., and S. Pond, 1982: Sensible and latent heat flux measurements over the ocean. J. Phys. Oceanogr., 12, 464–482, https://doi.org/10.1175/1520-0485(1982)012<0464:SALHFM> 2.0.CO:2.
- —, J. McWilliams, and S. Doney, 1994: Ocean vertical mixing: A review and a model with a nonlocal boundary layer parameterization. *Rev. Geophys.*, 32, 363–403, https://doi.org/10.1029/94RG01872.
- Lynn, R. J., and J. J. Simpson, 1987: The California Current System: The seasonal variability of its physical characteristics. *J. Geophys. Res.*, 92, 12 947–12 966, https://doi.org/10.1029/JC092iC12p12947.
- McCulloch, M., P. Spurgeon, and A. Chuprin, 2012: Have midlatitude ocean rain-lenses been seen by the SMOS satellite? *Ocean Model.*, **43–44**, 108–111, https://doi.org/10.1016/j. ocemod.2011.12.005.
- Muñoz Sabater, J., 2019: ERA5-Land hourly data from 1981 to present. Copernicus Climate Change Service (C3S) Climate Data Store (CDS), https://doi.org/10.24381/cds.e2161bac.
- Payne, A. E., and Coauthors, 2020: Responses and impacts of atmospheric rivers to climate change. *Nat. Rev. Earth Environ.*, 1, 143–157, https://doi.org/10.1038/s43017-020-0030-5.
- Price, J. F., 1979: Observations of a rain-formed mixed layer. J. Phys. Oceanogr., 9, 643–649, https://doi.org/10.1175/1520-0485(1979)009<0643:OOARFM>2.0.CO;2.
- Ralph, F., and M. Dettinger, 2011: Storms, floods and the science of atmospheric rivers. Eos, Trans. Amer. Geophys. Union, 92, 265–266, https://doi.org/10.1029/2011EO320001.
- —, and —, 2012: Historical and national perspectives on extreme West Coast precipitation associated with atmospheric rivers during December 2010. *Bull. Amer. Meteor. Soc.*, 93, 783–790, https://doi.org/10.1175/BAMS-D-11-00188.1.
- —, T. Coleman, J. Neiman, J. Zamora, and D. Dettinger, 2013: Observed impacts of duration and seasonality of atmospheric-river landfalls on soil moisture and runoff in coastal Northern California. *J. Hydrometeor.*, 14, 443–459, https://doi.org/10.1175/JHM-D-12-076.1.
- Ramon, J., L. Lledó, V. Torralba, A. Soret, and F. J. Doblas-Reyes, 2019: What global reanalysis best represents near-surface winds? *Quart. J. Roy. Meteor. Soc.*, 145, 3236–3251, https://doi.org/10.1002/qj.3616.
- Ramos, A. M., R. Roca, P. M. Soares, A. M. Wilson, R. M. Trigo, and F. M. Ralph, 2021: Uncertainty in different precipitation products in the case of two atmospheric river events. *Environ. Res. Lett.*, 16, 045012, https://doi.org/10.1088/1748-9326/abe25b.
- Ren, A. S., and D. L. Rudnick, 2021: Temperature and salinity extremes from 2014–2019 in the California Current System and its source waters. *Nat. Commun. Earth Environ.*, 2, 62, https://doi.org/10.1038/s43247-021-00131-9.
- Ren, L., and S. C. Riser, 2009: Seasonal salt budget in the northeast Pacific Ocean. J. Geophys. Res., 114, C12004, https://doi. org/10.1029/2009JC005307.
- Rudnick, D., 2016: California underwater glider network. Scripps Institution of Oceanography, Instrument Development Group, accessed 8 January 2020, https://doi.org/10.21238/S8SPRAY1618.
- —, K. Zaba, R. Todd, and R. Davis, 2017a: A climatology using data from the California Underwater Glider Network. Scripps Institution of Oceanography, Instrument Development Group, accessed 11 September 2020, https://doi.org/10.21238/ S8SPRAY7292.
- —, K. D. Zaba, R. E. Todd, and R. E. Davis, 2017b: A climatology of the California Current System from a network of

- underwater gliders. *Prog. Oceanogr.*, **154**, 64–106, https://doi.org/10.1016/j.pocean.2017.03.002.
- Schmitt, R., 2008: Salinity and the global water cycle. *Oceanogra*phy, **21**, 12–19, https://doi.org/10.5670/oceanog.2008.63.
- Schneider, N., E. Di Lorenzo, and P. P. Niiler, 2005: Salinity variations in the southern California Current. *J. Phys. Oceanogr.*, 35, 1421–1436, https://doi.org/10.1175/JPO2759.1.
- Seabird Scientific, 2016: How accurate is salinity measured by my CTD? What factors impact accuracy? https://blog.seabird. com/ufaqs/how-accurate-is-salinity-measured-by-my-ctd-what-factors-impact-accuracy/.
- Shields, C. A., and J. T. Kiehl, 2016: Simulating the Pineapple Express in the half degree Community Climate System Model, CCSM4. *Geophys. Res. Lett.*, **43**, 7767–7773, https://doi.org/10.1002/2016GL069476.
- Smyth, W., P. Zavialov, and J. Moum, 1997: Decay of turbulence in the upper ocean following sudden isolation from surface forcing. *J. Phys. Oceanogr.*, 27, 810–822, https://doi.org/10. 1175/1520-0485(1997)027<0810:DOTITU>2.0.CO;2.
- Soloviev, A. V., S. Matt, and A. Fujimura, 2015: Three-dimensional dynamics of freshwater lenses in the ocean's near-surface layer. *Oceanography*, 28, 142–149, https://doi.org/10.5670/oceanog.2015.14.
- SPURS-2 Planning Group, 2015: From salty to fresh—salinity processes in the upper-ocean regional study-2 (SPURS-2): Diagnosing the physics of a rainfall-dominated salinity minimum. *Oceanography*, 28, 150–159, https://doi.org/10.5670/oceanog.2015.15.
- Tarek, M., F. Brissette, and R. Arsenault, 2020: Evaluation of the ERA5 reanalysis as a potential reference dataset for hydrological modelling over North America. *Hydrol. Earth Syst.* Sci., 24, 2527–2544, https://doi.org/10.5194/hess-24-2527-2020.
- Thompson, E. J., J. N. Moum, C. W. Fairall, and S. A. Rutledge, 2019: Wind limits on rain layers and diurnal warm layers. *J. Geophys. Res. Oceans*, **124**, 897–924, https://doi.org/10.1029/2018JC014130.

- Tomczak, M., 1995: Salinity variability in the surface layer of the tropical western Pacific Ocean. J. Geophys. Res., 100, 20499– 20515, https://doi.org/10.1029/95JC01544.
- Vinogradova, N., and Coauthors, 2019: Satellite salinity observing system: Recent discoveries and the way forward. *Front. Mar. Sci.*, **6**, 243, https://doi.org/10.3389/fmars.2019.00243.
- Walesby, K., J. Vialard, P. Minnett, A. Callaghan, and B. Ward, 2015: Observations indicative of rain-induced double diffusion in the ocean surface boundary layer. *Geophys. Res. Lett.*, 42, 3963–3972, https://doi.org/10.1002/2015GL063506.
- Webster, P. J., C. A. Clayson, and J. A. Curry, 1996: Clouds, radiation, and the diurnal cycle of sea surface temperature in the tropical western pacific. *J. Climate*, **9**, 1712–1730, https://doi.org/10.1175/1520-0442(1996)009<1712:CRATDC>2.0.CO;2.
- Wijesekera, H., C. Pauson, and A. Huyer, 1999: The effect of rainfall on the surface layer during a westerly wind burst in the western equatorial Pacific. *J. Phys. Oceanogr.*, **29**, 612–632, https://doi.org/10.1175/1520-0485(1999)029<0612: TEOROT>2.0.CO;2.
- Williams, P., E. Guilyardi, R. Sutton, J. Gregory, and G. Madec, 2006: On the climate response of the low-latitude Pacific Ocean to changes in the global freshwater cycle. *Climate Dyn.*, 27, 593–611, https://doi.org/10.1007/s00382-006-0151-7.
- Wong, A. P. S., and Coauthors, 2020: Argo data 1999–2019: Two million temperature-salinity profiles and subsurface velocity observations from a global array of profiling floats. *Front. Mar. Sci.*, **7**, 700, https://doi.org/10.3389/fmars.2020.00700.
- Yu, L., 2011: A global relationship between the ocean water cycle and near-surface salinity. J. Geophys. Res., 116, C10025, https://doi.org/10.1029/2010JC006937.
- —, S. A. Josey, F. M. Bingham, and T. Lee, 2020: Intensification of the global water cycle and evidence from ocean salinity: A synthesis review. *Ann. N. Y. Acad. Sci.*, **1472**, 76–94, https://doi.org/10.1111/nyas.14354.
- Zhu, Y., and R. E. Newell, 1998: A proposed algorithm for moisture fluxes from atmospheric rivers. *Mon. Wea. Rev.*, 126, 725–735, https://doi.org/10.1175/1520-0493(1998)126
 0725:APAFMF>2.0.CO;2.